INFORMATION TO USERS

This manuscript has been reproduced from the microfilm master. UMI films the text directly from the original or copy submitted. Thus, some thesis and dissertation copies are in typewriter face, while others may be from any type of computer printer.

The quality of this reproduction is dependent upon the quality of the copy submitted. Broken or indistinct print, colored or poor quality illustrations and photographs, print bleedthrough, substandard margins, and improper alignment can adversely affect reproduction.

In the unlikely event that the author did not send UMI a complete manuscript and there are missing pages, these will be noted. Also, if unauthorized copyright material had to be removed, a note will indicate the deletion.

Oversize materials (e.g., maps, drawings, charts) are reproduced by sectioning the original, beginning at the upper left-hand corner and continuing from left to right in equal sections with small overlaps. Each original is also photographed in one exposure and is included in reduced form at the back of the book.

Photographs included in the original manuscript have been reproduced xerographically in this copy. Higher quality 6" x 9" black and white photographic prints are available for any photographs or illustrations appearing in this copy for an additional charge. Contact UMI directly to order.

UMI

A Bell & Howell Information Company
300 North Zeeb Road, Ann Arbor MI 48106-1346 USA
313/761-4700 800/521-0600

Properties

of a Two-Dimensional Low Density Electron System

Near the $B = 0$ Metal-Insulator Transition

by

DMITRI SIMONIAN

A dissertation submitted to the Graduate Faculty in Physics in partial fulfillment of the requirements for the degree of Doctor of Philosophy, The City University of New York.

1998

This manuscript has been read and accepted for the Graduate Faculty in Physics in satisfaction of the dissertation requirement for the degree of Doctor of Philosophy.

September 16, 1998
Date

Myriam P. Sarachik
Chair of Examining Committee

9/17/98
Date

Executive Officer

A. B. Fowler

A. Genack

J. Gersten

F. Smith

Supervisory Committee

THE CITY UNIVERSITY OF NEW YORK

ACKNOWLEDGEMENTS

All the experimental work which this Thesis is based on was done with the financial support of the United States Department of Energy.

I wish to express my gratitude to all people that made this work possible.

I am fortunate to have had a chance to be Myriam Sarachik's Ph.D. student. There is no doubt I have become a better physicist and (hopefully!) a better person, more tolerant and caring, as a result of that enormous amount of attention and guidance that I have received from Myriam. Her brilliant physical intuition and unfailing pursuit of the gist of every problem have defined the style of my approach to experiments. I am thankful to Myriam Sarachik for allowing me to work on the problems that were most appealing to me, for her encouragement, and sincere joy that she shared with me when the experimentalists' fortune smiled on us. At last, I would like to say that our group would not have been able to function at all without her ingenious optimism, that kept us all upbeat in the days of grossly insufficient funding.

Without Sergey Kravchenko, a Research Associate Professor in our group (now at Northeastern University in Boston, MA), this work would simply not have been done. Sergey's discovery in 1994 of the (theoretically "forbidden") metal-insulator transition in a two-dimensional system in the absence of a magnetic field, I believe, have made and will yet make many researchers busy. I benefitted enormously from the opportunity to work with him in this new area, in which, as it turned out, some spectacular effects had been waiting to be seen. Sergey introduced me to the field of two-dimensional physics and taught me some tricky experimental techniques peculiar to the study of high-mobility Si devices below 1 Kelvin.

I sincerely thank these two scientists for all that they have done for me.

I have my pleasure in thanking other people in Sarachik's group – Jonathan R. Friedman (now at the University at Stony Brook) and Snežana Bogdanovich (now at the University of Michigan), who I learned from during the early days of my tenure in the group, and who, together with Yicheng Zhong, expressed a lot of interest in my work, and created a very stimulating research environment. I am obliged to the Department of Physics machine shop foreman Mr. Joseph Altmann, for his having spent a lot of time with me on improving my designs.

Professor Robert Wheeler kindly shared with us silicon MOSFETs that accumulated in his Yale laboratory during years of fabrication. Professor Andy Kent of New York University let me use the wire bonding equipment in his lab, allowing me to prepare for measurements a dozen of working devices; he also introduced me to his OXFORD HELIOX^{VL} pumped ^{3}He system that was used in our tilted magnetic field experiment. I am delighted to have an opportunity to thank Peter Coleridge, V. Dobrosavljević, A. Efros, A. M. Goldman, Subir Sachdev, Dan Shahar, Len Tevlin, Chandra Varma, and R. W. Wheeler for valuable and enlightening discussions.

I am grateful to The City of New York for having become my adopted home town, thereby letting me continue work in physics.

I would like to acknowledge the contributions of the two people to whom I shall always be indebted – my high school teachers: of Physics – Mr. Anatoly Freedman, in Rīga, Latvia; of Mathematics – Ms. Raya Trotsenko, now at Ohr-Eliezer High School Yeshiva in Brooklyn. I wish to thank my old friends Dmitriy and Edith Mandel, for their unfailing belief in me. My wife Veronika needs to be thanked for this, and also for walking our dog alone in the night.

Finally, all that I have achieved has its source in love, determination and sacrifice of my parents.

LIST OF SYMBOLS AND ABBREVIATIONS

2D	Two-dimensions (-al)
DOS	Density of states
LL	Landau level(s)
MIT	Metal–Insulator Transition
MOSFET	Metal-Oxide-Semiconductor Field-Effect Transistor
QPT	Continuous Quantum Phase Transition

D	Electron diffusion constant at $T = 0$
d_{ox}	Oxide thickness; distance between the Gate and Si-SiO_2 interface
G	Conductance
g_v	valley degeneracy
$\bar{\kappa}$	average dielectric constant for electrons at the Si–SiO_2 interface
L_ϕ	Phase-breaking length
l_m	magnetic length equal to $\sqrt{\hbar c/eH}$
$l(\tau)$	Elastic mean free path (time)
$\lambda_F(k_F)$	Fermi wavelength (wavevector)
m^*	carrier effective mass
$\mu(n_s)$	density-dependent electron mobility
$n_{s(c)}$	Electron density (critical electron density)
r_s	Distance between carriers normalized by the effective Bohr radius.
τ_{SO}	Characteristic time between spin-orbit scattering events
V_g	Gate voltage applied between the Gate and 2D layer

v	number of electronic states in a Landau level, $v \equiv g_s g_v (eB/hc)$
ξ	correlation length near the quantum critical point
ξ_τ	correlation time near the quantum critical point

Contents

List of Figures

List of Tables

Chapter 1

INTRODUCTION

Although extensively studied since the mid-sixties [1], two-dimensional (2D) systems are still springing surprises on us [2]. Two dimensions are easier to visualize than three, yet it is in this subspace that some very fundamental electronic behavior in real systems – near absolute zero of temperature and in the absence of an external magnetic field – remains unexplained. In one special case, when *interactions between electrons* are small, a 2D system is believed to become an insulator as $T \rightarrow 0$, no matter how weak the *disorder potential* [3]. As a consequence, no metallic phase (and no MIT) is expected in this case.

The understanding of behavior at high magnetic fields in 2D systems is better: observations of the integer quantum Hall effect (QHE) has an explanation that rests on the existence of extended states, separated by states localized by disorder [4]. In cleaner systems exhibiting the fractional quantum Hall effect (FQHE), both disorder and interactions between electrons are included in an adequate theoretical explanation (for a recent review, see Ref.[5]).

The focus of our investigation here is the low-temperature behavior of the prototypical 2D system. We have studied inversion layers in Si MOSFET, clean enough to remain mobile (below 1 K) at low electron density $\approx 10^{10}$ cm^{-2}. This system provides

an experimental realization of a 2D *disordered* system where the *interactions* between electrons are very strong. Contrary to expectations [3], a $B = 0$ conducting phase was found [6] in samples with mobility greater than 1.5×10^4 cm^2/Vs at electron densities on the order of 10^{11} cm^{-2}. The observation of conducting behavior and a MIT in the absence of a magnetic field in a system [6] where both disorder and electron interactions are important, has no accepted theoretical explanation to date.

In this Thesis I present the experimental results of my work on a system that shows such anomalous behavior. We believe that several new significant observations that are reported here will provide clues for theorists trying to explain the $H = 0$ conducting behavior, and will prompt experimentalists to look for similar effects in other strongly interacting 2D systems.

Chapter 2 sets the stage for discussing the effects near this surprising transition in 2D: I introduce the well-known theoretical concepts for the electronic behavior in 2D systems, provide examples of the experimental tests of localization in two dimensions, review original measurements by Kravchenko and his collaborators, and discuss the essential physics near quantum phase transitions (QPT). The structure of Si MOSFETs and measurement techniques employed are described in Chapter 3. In Chapter 4 I present new experimental results on electronic transport near this transition. The results of Chapter 4 are discussed and compared to the existing theories in Chapter 5, and are followed by concluding remarks.

Chapter 2

ELECTRONIC BEHAVIOR IN TWO DIMENSIONS NEAR ABSOLUTE ZERO OF TEMPERATURE

In this Chapter I introduce theoretical concepts that are necessary for the understanding and interpretation of the experimental results: the behavior of non-interacting electrons in two dimensions and one-parameter scaling; existing theoretical treatments of the interacting problem, and quantum critical behavior. I also review two sets of experiments in 2D systems: early work that supports the $H = 0$ localization in 2D, and the original observations by Kravchenko *et al.* of the $B = 0$ MIT in Si MOSFETs.

2.1 Non-interacting electrons in two dimensions.

Let us start with an electron system in a crystal lattice with some amount of imperfections and assume for now that the interactions between electrons are negligible.[1] Later in this Chapter (see Equations 2.8, 2.9 and the discussion that follows) I provide estimates to show how realistic this assumption is. In the absence of thermal excitations, at $T = 0$, the electron system in a *perfect* lattice would be a perfect ($\rho = 0$) conductor (by virtue of Bloch's Theorem). At a finite temperature and in a real lattice, the electrons scatter off impurities, off phonons, and off each other. On the assumption that these scattering mechanisms are independent, the frequency of collisions is additive, hence the resistivity is a sum of all contributions:

$$\rho(T) = \rho_0 + aT^2 + bT^m, \tag{2.1}$$

where ρ_0 is a temperature-independent resistivity caused by lattice disorder, aT^2 is due to electron-electron scattering, and bT^m with $m = 3...5$ is due to electron-phonon scattering. As $T \to 0$, the last two scattering mechanisms become ineffective as the number of phonons and thermal excitations of the electron gas decreases at low T. Thus, collisions with the impurities in the real lattice account for the residual (*i.e.* in the limit of $T \to 0$) resistivity, ρ_0. Resistivity of the form of Equation 2.1 has been observed in good metallic films.[2] Systems that have *finite* resistivity in the limit of $T = 0$ will be called *metallic* in the rest of this work.

At very low temperatures and in systems with a sufficient amount of disorder (as in doped semiconductors, metal-oxide-semiconductor devices, semiconductor heterostructures *etc.*) the semiclassical description leading to Equation 2.1 becomes invalid. By treating non-interacting electrons semiclassically we overlook the fact that

[1] The rest of this Section deals with non-interacting electron systems.

[2] Strictly speaking, the $T = 0$ limiting behavior of very pure metallic films is correctly described by Eq.2.1 only due to finiteness of the film size.

electron wave functions *interfere* with each other. As will be shown below, quantum effects dominate the ultimate low-temperature behavior.

Multiple collisions of an electron with impurities are elastic; these collisions introduce phase shifts in electron wave functions without destroying phase memory. As a result of such events, an electron may return to its original position (making a *loop* in its trajectory), or diffuse away from it. It was shown, for example, in Ref. [7] that the probability of return is greater than the probability of diffusion, due to constructive interference of two Feynman paths along the loop that differ only in direction of the electron wave-vector (time-reversed paths). This effect reduces the diffusion of electrons and enhances the resistivity of the system, leading to *localization* of carriers.

Since inelastic scattering processes (*e.g.* electron-electron or electron-phonon) involve energy transfer, they destroy phase-coherence of the electron Feynman paths. Thus, the correction $\Delta\sigma$ to the conductivity due to the interference effect should become smaller as the temperature increases, and ultimately vanish at high T, as the probability of inelastic scattering events increases. The authors of Ref.[7] derived the functional forms of $\Delta\sigma$ for dimension d of a system:

$$\Delta\sigma \sim -\begin{cases} \frac{e^2}{\hbar l} - \frac{e^2}{\hbar L_\phi} & \text{if } d\text{=3, } [\sigma]\text{=(Ohm cm)}^{-1} \\ \frac{e^2}{\hbar} \ln\left(\frac{L_\phi}{l}\right) & \text{if } d\text{=2, } [\sigma]\text{=Ohm}^{-1} \\ \frac{e^2 L_\phi}{\hbar} & \text{if } d\text{=1, } [\sigma]\text{=(Ohm/cm)}^{-1} \end{cases} \tag{2.2}$$

The units naturally follow from the dimension-dependent definitions of conductivity, for example, in 2D σ = conductance $\times \frac{\text{length}}{\text{width}}$, and has the unit of Ohm^{-1}. In the above, l is the elastic mean-free path and L_ϕ is the (temperature- dependent) dephasing length arising from inelastic scattering: $L_\phi \propto T^{-p/2}$, where p depends on the scattering mechanism.

It can be seen from Equation 2.2 that the negative correction due to interference, $\Delta\sigma$, grows with increasing disorder (decreasing elastic mean-free path l) in 3D and

2D, and with decreasing temperatures (increasing dephasing length L_ϕ). Let us consider the specific dependences of the corrections on temperature: In 3D $\Delta\sigma$ tends to a *finite* value, while in 2D and 1D it *diverges* as $T \to 0$. By examining $\Delta\sigma(T)$ dependences in different dimensions, one can notice[3] that the ultimate $T = 0$ behavior of a disordered system in 2D and 1D cannot be metallic, since the conductivity decreases indefinitely with decreasing temperature (see Equation 2.2). The non-interacting disordered electron system in 2D should, therefore, be an *insulator*, with $\sigma \to 0$ ($\rho \to \infty$) as $T \to 0$. Support for this result is provided by the scaling theory of localization, discussed in Section 2.2.

So far we considered quantum corrections to the conductivity of a disordered system at low T when no external magnetic field was applied. In the presence of a magnetic field, the electron wave function interference gives rise to different forms of magnetoconductance, depending on whether there are any scattering channels present that lead to changes of electron spin direction (*e.g.*, spin-orbit scattering). The experimentally measured response to a magnetic field is a valuable complement to the temperature dependence of the conductivity. In Table 2.1 quantum corrections to the conductivity in the presence of an external magnetic field H are shown for two different scattering processes in which (otherwise non-interacting) electrons are involved. The physics leading to these corrections is as follows.

Spinless: In this case, magnetic flux threading a closed electron trajectory introduces a phase shift that suppresses constructive interference of time-reversed paths, weakening the localizing effect of wavefunction interference: $\Delta\sigma > 0$. τ_B is the time it takes an electron to diffuse over a distance comparable to the magnetic length, $\tau_B = l_m^2/2D = (1/2D)\hbar c/eH$. Suppression of weak localization sets in when $\tau_B \leq \tau_\phi$, which gives the estimate for the smallest field, $H \sim 30$ Oe.

[3]The argument is not strict, since the functional forms of corrections (2.2) are valid for small corrections, $\Delta\sigma \ll \sigma$.

Electron scattering is:	Form of $\Delta\sigma \equiv \sigma(T,H) - \sigma(T,0)$	Observed in experiments on	Relevant range of H
spinless	$\Delta\sigma \approx e^2/(2\pi^2\hbar)[\Psi(0.5 + 0.5\tau_B/\tau_\phi) + \Psi(0.5 + 0.5\tau_B/\tau)]$ [8, 9]	e-inversion layers in MOS devices with $\mu \sim 10^3$ cm^2/(Vs) at densities $\sim 5 \times 10^{12}$ cm^{-2} [10]	Positive correction to conductivity appears for $H > \frac{\Phi_0}{D\tau_\phi} \approx 30$ Oe at 0.1 K
spin-orbit	$\Delta\sigma \approx -e^2/(2\pi^2\hbar)\frac{1}{24}(\tau_\phi/\tau_B)$, if $\tau_{SO} << \tau_\phi << \tau_B$ [9]	Mg films covered with submonolayers of Au [11]; Cu films [12]	Negative correction due to SO persists up to $H < \frac{\Phi_0}{D\tau_{SO}} \sim 200$ Oe for 1% of atomic layer of Au on a Mg film

Table 2.1: Quantum corrections to the conductivity in the presence of an external magnetic field H, for the case of spinless and spin-orbit scattering mechanisms.

Spin–orbit scattering: In the presence of strong ($\tau_{SO} << \tau_\phi$) spin-orbit interaction the low-field correction to conductivity becomes negative. The low-field condition for fields at which the conductivity correction has a negative sign is: $\tau_\phi << \tau_B$ This effect is most clearly explained [13] by considering interfering time-reversed Feynman paths along the loop as two actual interfering particles. These two particles can be in four states characterized by the total spin: $S = 1$ (three states: $|S_z = -1\rangle, |S_z = 0\rangle$, and $|S_z = +1\rangle$) and $S = 0$. The $S = 0$ state "carries no information about the spin" [13], and therefore, constructive interference of orbital parts of electron wavefunctions is cut off at times τ_ϕ, just as in the spinless case.[4] However,

[4]Because of the condition $\tau_{SO} << \tau_\phi << \tau_B$, the other $S \neq 0$ states decay with a characteristic

electrons in the $S = 0$ state have opposite spins. Thus, *constructive* interference of orbital parts leads to the *destructive* interference of *total* wavefunctions that results in delocalization. Application of a magnetic fields introduces a phase shift that weakens this delocalizing effect of the destructive interference. Thus, the correction to conductivity in the presence of SO, has a negative (localizing) sign, $\Delta\sigma < 0$.

As the applied magnetic field gets larger, the time τ_B decreases. Spin-orbit scattering becomes unimportant when $\tau_B << \tau_{SO}$, because the dominant dephasing is caused by the magnetic field under this condition. Therefore, the effect of SO is suppressed by large magnetic fields, *i.e.* when $\tau_B >> \tau_{SO}$. At such fields the conductivity correction changes sign to positive, so that the field-induced delocalization takes over.

(temperature-independent) time $\sim \tau_{SO}$, and do not have a temperature-dependent contribution.

2.2 One-parameter scaling theory of localization.

Let us review the basic consequences of the scaling theory of localization that are necessary for the understanding of experimental results in 2D systems. In the limit of $T = 0$, the dephasing length becomes very large, $L_\phi \to \infty$, and the interference cutoff is provided by the physical size of the sample, L. The hypothesis of scaling invariance [14, 3] states that at $T = 0$ the conductance G of the system is the *only* quantity that determines the change in the behavior of the system with changing size L. If the size of the system changes by a factor of $1 + \alpha$, the scaling invariance condition can be written in the form[5]

$$G((1+\alpha)L) = f(\alpha, G(L)). \tag{2.3}$$

On differentiation with respect to α we get:

$$L\, dG/dL = (\partial f/\partial \alpha)\Big|_{\alpha=0} \tag{2.4}$$

Now if we introduce a new function of conductance G only,
$\beta(G) \equiv G^{-1}(\partial f/\partial \alpha)\Big|_{\alpha=0}$, Equation 2.4 will read:

$$\partial \ln G/\partial \ln L = \beta(G). \tag{2.5}$$

Consider the asymptotic behavior of the newly introduced function $\beta(G)$ at large conductance G. In this limit Ohm's law can be applied:

$$G = \sigma\frac{S_\perp}{L} = \sigma\begin{cases} L^2/L \equiv L, & d=3 \\ L/L \equiv 1, & d=2 \\ L^{-1}, & d=1, \end{cases} \tag{2.6}$$

where $S_\perp$ is the size of the cross-section of the 3, 2, or 1-dimensional conductor. From Equation 2.5 it follows that $\beta(G) \approx d-2$ (in the limit of large G). Now consider the

[5] In the following, I discuss the scaling argument following the lines of Ref. [13, p. 195; see references therein.]

other extreme – very small G. In this limit electrons are localized by disorder. That means that electron wave functions have a certain characteristic extent; at $T = 0$ an electron is bound to a region in space characterized by the *localization length* ξ. For small sample size $L \ll \xi$ the electrons "may not know" that they are localized, however, as L increases, the finiteness of the localization length leads to the decrease of total conductance. Formally this can be expressed as follows:

$$G \sim G_0 \exp(-L/\xi), \text{ where } G_0 = e^2/(\pi^2\hbar) \tag{2.7}$$

This form G is consistent with the scaling invariance idea [3]: the conductance G of the system is, indeed, the only quantity that determines the change in the behavior of the system with changing size $L \to (1+\alpha)L$: $G((1+\alpha)L)/G_0 = e^{(-L(1+\alpha)/\xi)} = (G(L)/G_0)^{1+\alpha}$. From Equation 2.7 we obtain the asymptotic form of β at small G: $\beta(G) \sim \ln(G/G_0)$.

Now, having the asymptotes of $\beta(G)$, $\beta(G) \approx d-2$ as $G \to 0$, and $\beta(G) = \ln(G/G_0)$ as $G \to \infty$, and assuming monotonic behavior of β for the intermediate values of G, we arrive at the well-known $\beta(G)$ dependences in 1, 2, and 3 dimensions shown in Figure 2.2. It can be seen from this figure that in one and two dimensions $\beta(G)$ is always negative, implying that the conductance decreases with increasing size L, which means that the system is *localized*, as was discussed above.

What consequences does this result, obtained in the assumption that $T = 0$, have for the electronic transport at *finite* temperatures? At $T = 0$ the quantum effects that give rise to localization are cut off by the sample size L. When $T > 0$ these quantum effects are cut off at the dephasing length L_ϕ introduced in Section 2.1. This length is much smaller than L for macroscopic samples. It takes on the role of the physical sample size L: L_ϕ should be substituted for L at $T > 0$. Thus, for finite T the consequence of $\beta(G) < 0$ in 1D and 2D is: conductance G decreases with increasing size L_ϕ, or with decreasing T. This is characteristic of an *insulating*

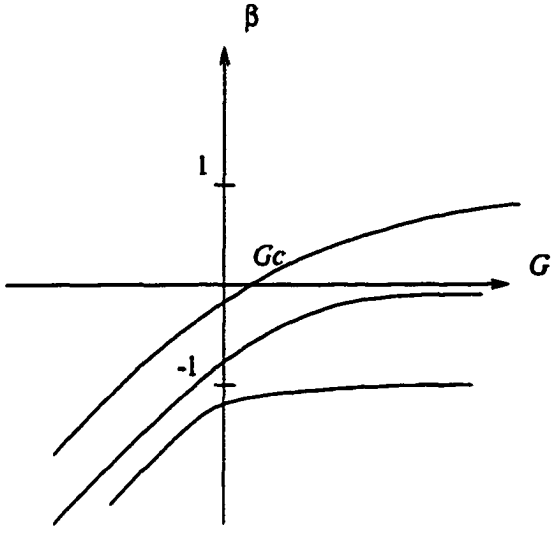

Figure 2.1: β-function plotted versus conductance G. Metallic behavior (and the MIT) in a non-interacting disordered system are only possible in 3D; G_c is the *critical* conductance separating insulating ($\beta(G) < 0$) phase from metallic ($\beta(G) > 0$) phase. (see the text following Eq.2.5 on page 9)

behavior. The scaling invariance hypothesis has led us to the same conclusion as was made at the end of Section 2.1 based on examination of the quantum corrections to the conductivity due to interference: in 1D and 2D a non-interacting electron system must become an insulator in the limit of $T = 0$.[6] In three dimensions, $\beta(G)$ crosses the abscissa at a point $G = G_c$ (see fig.2.2), which separates *insulating* behavior, $\beta(G) > 0$ for $G < G_c$, from *metallic* behavior, $\beta(G) > 0$ for $G > G_c$ [7] We will call G_c

[6] We stress here again that the localization can only be observed experimentally if the sample size $L \gg \xi$. This explains why very clean metallic films appear to have a finite residual resistivity at low enough T (i.e. appear to remain delocalized at $T = 0$): the enormous localization length in very clean samples is cut off by the physical size.

[7] It follows from $\beta(G > G_c) > 0$ that in the range $G > G_c$ the conductance increases with the increasing size L at $T = 0$. At finite T, $L \to L_\phi$, so G increases with increasing L_ϕ (*i.e.* with

the *critical* conductance of the metal-to-insulator transition (MIT). In Section 2.4 we will see what characterizes the electronic transport in the vicinity of an MIT at low temperatures. For the understanding of the experimental results to follow, the most important conclusion of this Section is that in two dimensions, in the absence of an external magnetic field a non-interacting system is an insulator at $T = 0$, regardless of the value of G.

This result has been tested on many 2D systems and had been regarded as a very robust one for almost two decades. The logarithmic temperature dependence of resistivity of the form of Equation 2.2 (leading to an insulator at $T = 0$) has been found in weakly disordered metallic films with resistivity as low as 20 Ohm/□ (for example, in Cu films [15]), and in much more disordered inversion layers in Si MOSFETs with resistivities as high as 10 kOhm/□ at electron densities on the order of $n_s \sim 5 \times 10^{12}$ cm^{-2} [16]. At larger resistivities, early studies have shown (*e.g.*, Ref.[17]) a crossover to strongly localized behavior, characterized by an exponential growth of ρ with decreasing temperature. Insulating behavior at any amount of disorder, consistent with the assertion of the scaling theory, has been recently reported for electrons in n-typeGaAs/AlGaAs heterostructures [18].

We have been so far deliberately overlooking the fact that electrons (or holes) in 2D layers do interact with each other. In 2D the kinetic energy of electrons near $T = 0$ is:

$$\epsilon_F = \pi\hbar n_s/(g_v m^*) \propto n_s, \tag{2.8}$$

and the energy of the unscreened Coulomb interaction between carriers is:

$$\epsilon_{ee} = e^2 n_s^{\frac{1}{2}}\sqrt{\pi}/\bar{\kappa} \propto n_s^{\frac{1}{2}}. \tag{2.9}$$

The ratio ϵ_{ee}/ϵ_F is proportional to $n_s^{-\frac{1}{2}}$, and must be small for the system to be considered non-interacting or weakly-interacting. In the experiments on (100) inver-

decreasing temperature). This is characteristic of ***metallic*** behavior.

sion layers in Si at electron densities on the order of $n_s \sim 5 \times 10^{12}$ cm^{-2} [17, 16], $\epsilon_F \approx 30$ meV and $\epsilon_{ee} \approx 70$ meV, and this ratio is on the order of 2. It is obvious, therefore, that the non-interacting picture must be modified to include the effects of interactions between carriers.

2.3 Interacting electrons in two dimensions

The gist of the two previous Chapters can be summarized as follows: in the zero-temperature limit the non-interacting 2D system is an insulator, regardless of the amount of disorder. The presence of spin-orbit scattering has a delocalizing effect on a weakly disordered system (as was argued in the caption to Table 2.1).

Let us now consider systems in which spin-orbit interactions are unimportant (like Si MOSFET), and summarize what is known about the modifications that interactions between carriers may introduce.

The perturbative calculation [19, 20] for a weakly disordered ($l \gg \lambda_F$) system shows that exchange interactions between weakly interacting electrons result in an increase of the electron velocity at the Fermi level by an amount on the order of $e^2/\hbar$. Since the density of states is inversely proportional to the electron velocity, the interactions lead to a negative correction for the DOS and, as a consequence, to the conductivity. This correction has the following form in 2D:

$$\sigma(T) - \sigma(T') = (1 - F)\frac{e^2}{2\pi^2\hbar} \ln \frac{T}{T'}, \tag{2.10}$$

where $0 < F < 1$ characterizes screening of the interactions between carriers; $F \to 0$ for the unscreened interaction. The negative sign of this correction tells us that a weakly localized (by disorder) electron system in 2D, is further localized by weak electron interactions.

In the other limit (strong electron interactions), weakly disordered electrons are

believed to crystallize in a Wigner solid. The Wigner solid is an arrangement of electrons which is energetically more favorable than the Fermi liquid. The gain in interaction energy in the Wigner crystal phase is a consequence of an ordered configuration of electrons. The crystallization thus relies on the minimization of the energy of Coulomb interactions, and should occur at low densities, n_S, at which the Coulomb interactions dominate the kinetic energy (compare ϵ_F with ϵ_{ee} in Equations 2.9 and 2.8), or, alternatively, at high values of $r_s \equiv r_{ee}/a_B$, the inter-electron distance normalized by the effective Bohr radius $a_B \equiv \hbar^2/(m^*e^2)$[8]. Estimates of the critical value of r_s at which the formation of the crystal occurs vary widely [1], from 5 to 5×10^2, and it is not clear how the disorder affects this value.

Several experimental observations suggest that at low T the Wigner crystal actually exists at high-magnetic fields in inversion layers in Si [21, 22], and in 2D layers in GaAs/AlGaAs heterostructures [23, 24]; however, this question is not fully resolved. Weak disorder pins the crystal, resulting in a strongly insulating state as $T \to 0$. In the limit of very high disorder, the crystal should yield to single-particle (Anderson) localization, and the $T = 0$ state is an insulator again. It thus follows that, for weak interactions (single particle localization), and in the case of strong interactions but weak disorder (Wigner crystallization), the interacting 2D system must remain an insulator. The reader must surely be convinced by now that there was little expectation of finding a metal in a 2D system of electrons!

Before I go on to describe the experimental observations of Kravchenko and his coworkers [6, 25], I propose to map most of the types of low-temperature electronic behavior discussed above in 2D electron layers in semiconductors onto a convenient empirical phase diagram. There is undoubtedly a significant amount of evidence that disorder on the one hand, and electron interactions on the other hand, are the two im-

[8] r_s is a dimensionless quantity, proportional to the relative strength of Coulomb interactions, ϵ_{ee}/ϵ_F

portant parameters that govern the low-temperature behavior. How to extract them separately from the experimental data is not an obvious question. One traditionally characterizes the disorder in a 2D sample by the maximum *carrier mobility*, which is defined as a conductivity per unit charge density of carriers, and is usually specified at liquid helium temperature, $T = 4.2$ K[9].

$$\mu^{max} \equiv max\left(\mu(n_s)\right) = max\left(\frac{\sigma_{xx}}{en_s}\right) \tag{2.11}$$

The strength of interactions can be characterized by the inverse square root of the electron density, as seen from Equation 2.9. In Figure 2.3 (drawn for Si inversion

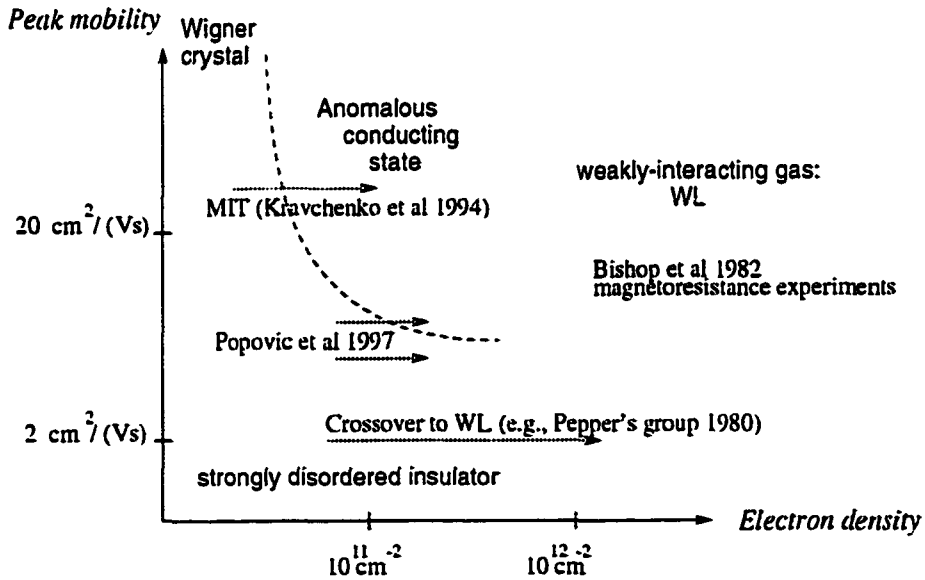

Figure 2.2: An experimentalist's "phase diagram" of the 2D electron system in Si MOS in the interactions—disorder phase space. The disorder grows with decreasing sample mobility. Relative strength of Coulomb interactions between electrons grows with decreasing density. See text for details.

[9]Details concerning this definition and experimental determination of sample mobility are given in Section 3.3 on page 29

layers), the peak electron mobility $\mu^{max}_{T=4.2K}(n_s)$ characterizes the disorder, and the electron density characterizes the relative strength of interactions.[10] Let us consider various well-understood limits of this phase diagram.

1. In the range of high electron densities we find ourselves in the weakly-interacting regime, because $\epsilon_F > \epsilon_{ee}$ (in the case of 2DEG in Si, this condition is satisfied for $n_s \gg 10^{12}$ cm^{-2}. In this limit, at moderate values of disorder (as in some of the MOSFET samples in Ref.[10, 17]) one observes weakly insulating behavior, with the theoretically anticipated logarithmic corrections. This corresponds to the far-right side of the phase diagram. In the low-mobility extreme, where $\mu \sim 2,000 \ldots 5,000$ cm^2/(Vs)), the system is a strongly disordered insulator at low n_s, and crosses over to WL as the electron density is increased [17].

2. In the range of low electron densities (strong interactions), the 2D system is believed to become a Wigner solid, if the disorder is weak. This corresponds to the upper-left corner of the diagram.

3. The most interesting region of the diagram is the region of high peak mobilities ($\mu \sim 15,000 \ldots 40,000$ cm^2/(Vs), and *intermediate* densities ($n_s \approx 10^{11}$ cm^{-2}). There is no accepted theoretical treatment of the low-temperature electronic behavior in this regime, because perturbations are not small: although the interactions are the dominant energy scale in this regime, $\epsilon_{ee} \sim 15\epsilon_F \approx 10$ meV, the Fermi energy and the disorder (the Fermi wavelength and the elastic scattering length) are comparable: $l \sim \lambda_F$. It is precisely in this regime that

[10] It should be noted that electron density affects not only interactions, but also the disorder. For example, in the non-interacting limit, the disorder potential is better screened for larger ratios of $k_F/q_{sc} \propto (n_s)^{\frac{1}{2}}$, that is, for larger electron densities. Here q_{sc} is the screening wavenumber, which in a non-interacting 2D system is equal to $(2\pi e^2/\bar{\kappa})\partial n_s/\partial \epsilon_F$.

the unexpected $H = 0$ conducting behavior in 2DEG in MOSFETs was observed [6, 25].

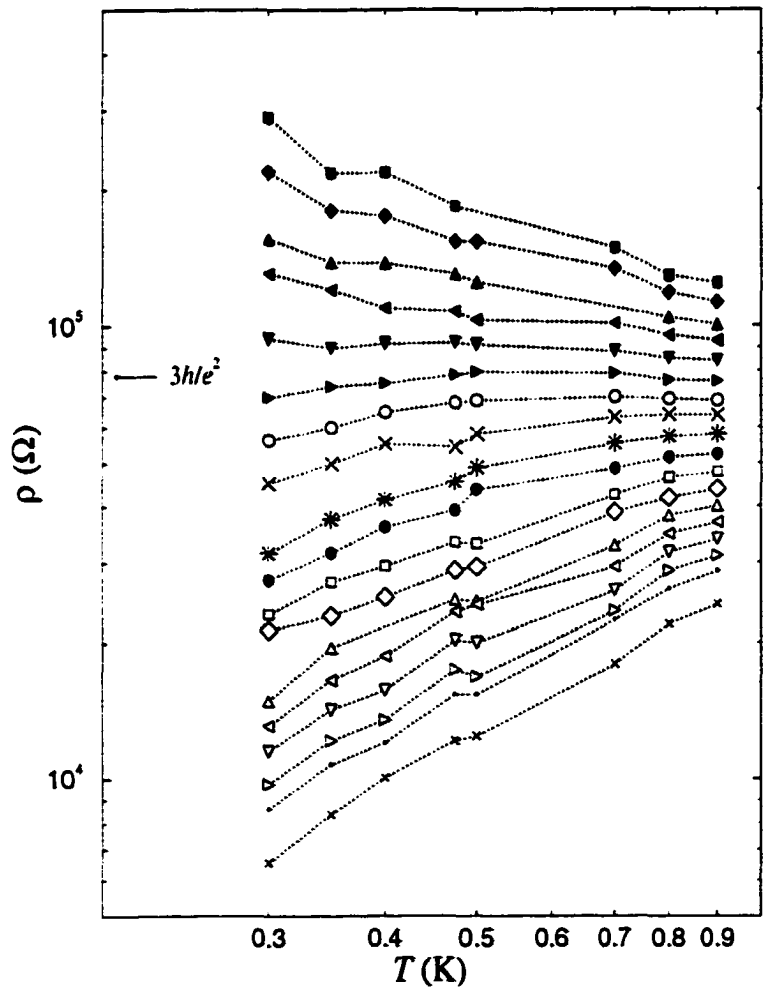

Figure 2.3: Ohmic resistivity measured on a high-mobility sample $\mu^{max}_{T=4.2\ K} \approx 24,000\ \mathrm{cm}^2/(\mathrm{Vs})$ at several electron densities around the metal-insulator transition. The data essentially reproduce the original results of Ref.[6]. Each data point is a result of an IV measurement, and of $I \to 0$ extrapolation of V/I. See text for details.

Figure 2.3 shows the ohmic resistivity as a function of temperature of a sample with maximum mobility $\mu^{max} = 24{,}000$ cm^2/(Vs), for electron densities between 7.92×10^{10} cm$^{-2} < n_s < 9.57 \times 10^{10}$ cm^{-2}. These measurements were done as a part of the scaling analysis in Section 4.2, and they essentially reproduce the first observations of Kravchenko *et al.* Two distinct regimes are obvious in Figure 2.3: for $n_s < n_c 8.47 \times 10^{10}$ cm^{-2} the behavior is insulating-like: the resistivity grows with decreasing temperature. For $n_s > n_c$ the resistivity monotonically decreases with temperature, and the behavior appears metallic. The temperature-independent value of the resistivity for the curve that separates the two types of behaviors (at $n_s = n_c$) is close to $3h/e^2 \approx 77.4$ kOhm/□, and was shown to be insensitive to variations of disorder in different high-mobility samples[11].

These findings suggested to the authors of Refs. [6, 25] that they had observed a true metal-insulator transition. They demonstrated that the resistivity near the transition scaled with the temperature, which further supported this possibility. Scaling is one of the signatures of behavior near a phase transition. I review the ideas of finite-size scaling near a quantum phase transition in the following Section.

2.4 Signatures of the quantum critical behavior.

In Chapter 4 I will present new experimental data that supports the possibility that the transition in an interacting 2DEG [6, 25] discussed in the previous Section is in fact a continuous quantum phase transition (QPT) between one quantum-mechanical ground state of the system (metallic state) and the other (insulating state). Since a quantum phase transition is a transition between different ground states of the system, it occurs in the limit of zero temperature, and is driven by a change of some

[11] This value is the same, for example, for samples with the high mobilities varying by as much as a factor of two at 4.2 K [6]

variable in the Hamiltonian of the system [26, see also references therein]. Magnetic field – driven [27, 28], or disorder – driven [29] superconductor–insulator transitions in thin superconducting films, filling factor – tuned transitions between Hall plateaus in quantum Hall samples, MITs in doped semiconductors (3D) [30, and references therein], —are some examples of quantum phase transitions. On the other hand, transitions driven by changes in temperature, like metal–superconductor transitions occurring at finite T_c are not.

It can be shown [26] that the behavior of a d–dimensional system at the quantum critical point at $T = 0$ is equivalent to the behavior of a $d + 1$–dimensional (d spatial directions + one time direction) system near the classical critical point. The existence of a diverging correlation length at the classical critical point (*e.g.* at the metal–superconductor transition occurring at a finite temperature) thus leads to the existence of a spatial correlation length ξ, plus a correlation length in the time direction (that is, correlation time) ξ_τ. In the vicinity of a $T = 0$ quantum critical point, the correlation lengths in space and time diverge as follows:

$$\xi \propto |\delta|^{-\nu} \tag{2.12}$$

$$\xi_\tau \propto \xi^z, \tag{2.13}$$

where ν is the correlation length exponent, z is the dynamical-scaling exponent, and $\delta \equiv (K - K_c)/K_c$ is a normalized distance to the critical point. K is some coupling (filling factor in the case of transitions between QH plateaus [26, section IV], dopant concentration [30] or uniaxial stress [31] in the case of MITs in bulk semiconductors, ratio of the Josephson coupling to the charging energy of the junction in Josephson junction arrays [32] *etc.*) that measures the approach to the critical point.

The effect of a non-zero temperature on the behavior of the system undergoing a $T = 0$ QPT is to introduce a finite size along the time direction, which equals $\hbar/(k_B T)$. The interplay between the correlation time, ξ_τ, and the temperature–induced finite

size in the time direction, $\hbar/(k_B T)$, fully describes the behavior of the system in the vicinity the quantum critical point. Within the quantum-critical region[12] [34] the temperature response of the resistivity is described by the principles of finite-size scaling [35, 34], which gives the following scaling form for the dc resistivity in the ohmic regime in two dimensions:

$$\rho(T) = \tilde{f}\left(\frac{\hbar/(k_b T)}{\xi_\tau}\right) \equiv f\left(\frac{\delta}{T^{\frac{1}{\nu z}}}\right) \tag{2.14}$$

This scaling form implies that the temperature-dependent resistivity curves $\rho(T)$ corresponding to different K's, can be brought into coincidence when the temperature is divided by an appropriate parameter $T_0(K)$, different for each curve. The scaling parameter can thus be determined empirically from the data, and *must* vary with K according to:

$$T_0 \propto \left|\frac{K - K_c}{K_c}\right|^{\beta} \equiv |\delta|^{\beta} \tag{2.15}$$

with the same exponent $\beta \equiv \nu z$ on *both* sides of the transition: for $\delta > 0$ and $\delta < 0$.

It was first shown in Ref. [25] that the resistivities measured near the unexpected critical point in strongly-interacting 2DEGs in Si MOSFETs do obey scaling of the form of Equation 2.14 expected in the vicinity of a quantum critical point. The exponent β in Equation 2.15[13] determined separately on both sides of the transition yields the following values [25]: $\beta = 1.60 \pm 0.1$ on the insulating side, and $\beta = 1.62 \pm 0.1$ on the metallic side. It is evident, therefore, that finite-size scaling near the QPT does indeed describe the behavior of a strongly interacting 2DEG in MOSFETs.

The scaling form of Equation 2.14 is valid for a dc ($\omega \to 0$) measurement of the resistivity in the linear regime ($E \to 0$). Finite ac frequency ω [36], or finite

[12]The quantum-critical region is the (temperature-dependent) neighborhood of the $T = 0$ critical point within which $k_B T$ is the only energy scale in the problem. The critical region is, therefore, set by the condition that $k_B T$ is much larger than the energy associated with the deviation from the critical point $K - K_c$ [33]

[13]with the electron density n_s taking on the role of K, so that $\delta = (n_s - n_c)/n_c$

measuring voltage, E×sample length, introduce other relevant energy scales that modify the scaling form 2.14.

At $T = 0$ the energy scale associated with the finite measuring field E, can be estimated to be eEL_E, where L_E is the characteristic length scale, associated with the field E [26, p.327]. If we now recall that the system is very close to the critical point, then it follows that L_E is the only length scale present, and thus, the characteristic time must scale according to Equation 2.13: L_E^z. From $eEL_E \sim \hbar/(L_E^z)$, one obtains: $L_E \propto E^{-1/(z+1)}$. Thus, at $T = 0$ electrons acquire an energy equal to $eEL_E = eE \cdot E^{-1/(z+1)} \equiv eE^{z/(z+1)}$. We now can modify the finite-size scaling law for the case of dc measurement of the resistivity *beyond* the ohmic regime at the lowest temperature (strictly speaking, at $T = 0$) in the following way. The behavior of the system in the vicinity of the quantum critical point is again fully described by the interplay between the correlation time, $\xi_\tau \propto |\delta|^{-\nu z}$, and the electric field–induced finite size in the time direction, $\hbar/(eE^{z/(z+1)})$, so we get:

$$\rho(T) = \tilde{f}\left(\frac{\hbar/(eE^{z/(z+1)})}{\xi_\tau}\right) \equiv f\left(\frac{\delta}{E^{\frac{1}{\nu(z+1)}}}\right) \tag{2.16}$$

It should be kept in mind that the scaling law (Equation 2.16) above holds for "strong" electric fields, *i.e.* at the lowest experimentally accessible temperature, and the thermal energy $k_B T$ must be significantly lower than the energy scale associated with the measuring field E. Two series of experiments on the same system undergoing a QPT– measurements of ohmic resistivity as a function of T, and nonlinear resistivity as a function of E – allow separate determination of the scaling exponents ν and z. This analysis has been done, for example, for the case of the quantum Hall liquid–insulator transition [37], and for the superconductor–insulator transition in disordered thin films [28]. Experimental study of the low-T nonlinear resistivity in a high-mobility strongly interacting gas in Si MOSFETs, presented in Chapter 4 is therefore of interest for two reasons: it will provide further evidence – if the nonlinear scaling

of the form of Equation 2.16 proves to hold – for a true QPT in our system, and will allow separate determination of the scaling exponents ν and z.

With this I conclude the background information needed to understand the experimental results presented in Chapter 4 on page 36.

Chapter 3

THE SYSTEM AND MEASUREMENT TECHNIQUES.

The experiments were done on a prototypical realization of a 2D system - electrons at the interface between oxide and semiconductor in Silicon-Oxide-Semiconductor Field Effect Transistors (MOSFETs). In the following Chapter, I outline the devices' structure and physical characteristics, then present the measurement techniques and the method of characterization. The experimental challenges that one meets in the course of investigating these devices at low densities and below 0.5K are outlined at the end of this Chapter.

3.1 The prototypical 2D disordered system: Si MOSFET

The Si MOSFET had been known as the work horse for experiments in two dimensions [1] until the near-million mobilities were achieved in GaAs/AlGaAs heterostructures [4]. It is interesting that although such high mobilities made the observation

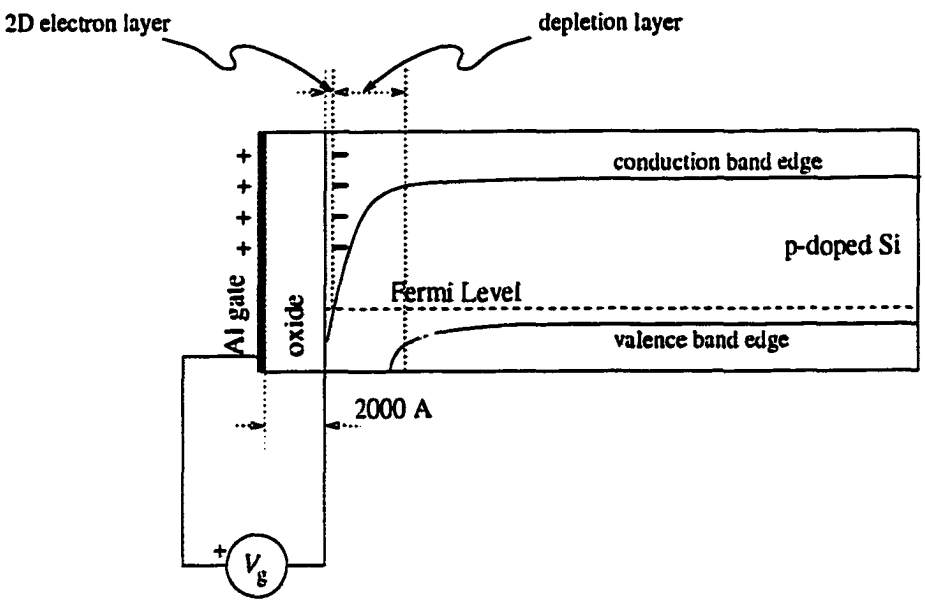

Figure 3.1: Silicon MOS field-effect transistor. Application of a positive gate bias V_g charges the capacitor formed by the gate and the surface of the p-doped Si substrate, creating a negatively charged depletion layer. Once the gate voltage is strong enough, $V_g > V_T$, *i. e.* the conduction band bottom is below the Fermi level, the 30 to 100Å–thick inversion layer of 2D electrons electrons is formed at the Si—SiO_2 interface.

of other novel effects possible (*e.g.*, fractional QHE), no unexpected anomalies at $H = 0$ were seen in n-type GaAs/AlGaAs.[1] The material parameters in Si MOS devices — comparatively low dielectric constant $\kappa \approx 8$, high effective electron mass $m^* = 0.19m_e$, and the presence of an additional two-fold valley degeneracy $g_v = 2$, — all contribute to increasing the relative importance of ϵ_{ee}, which make this system unique for studying the effects caused by the strong Coulomb repulsion of the carriers.

A MOSFET is schematically shown in Figure (3.1). A 2×10^{-5}cm-thick oxide

[1]We attributed this to smallness of interactions-to-kinetic energy ratio in n-type GaAs/AlGaAs as compared to Si MOSFETs, see estimates in Section 2.3 on page 13.

layer is grown on a p -type silicon substrate, on top of which a metallic gate is deposited. By applying a variable positive DC voltage to the gate, V_g, the electrons from the bulk can be attracted to the interface, and the bottom of the conduction band near the surface of Si is bent downward [1]. Thus the negative charge (the depletion layer) is formed in the region of significant band-bending (see Figure 3.1). Once the gate voltage is high enough that the conduction band edge is below the Fermi level ϵ_F, a 2D layer of electrons will be formed at the interface, where electrons are spatially confined to the surface of Si by the potential well[2], but are free to move in the directions parallel to the interface. One can see that there are no states at the Fermi level anywhere except in the region very close to the surface of Si; the actual spatial extent (along the normal to the surface) of an electron's wavefunction is 30 to 100Å, depending on the value of V_g. We can think of the gate voltage charging a capacitor between the gate and Si—SiO_2 interface; thus the higher V_g, the more surface electrons are induced, *i.e.* the higher their surface density n_s:

$$n_s = k(V_g - V_T), \tag{3.1}$$

where V_T is a threshold voltage which will be determined experimentally in Section 3.3; k is the constant of proportionality in units of $(\text{V cm}^2)^{-1}$. Typically, $k = 1.1 \times 10^{11}$ $(\text{V cm}^2)^{-1}$ for a 2000Å-thick oxide.

In the samples studied here, the surface of silicon is a (100) surface. The six-fold degeneracy of electron states in the conduction band of bulk Si is partially removed by electron confinement to the (100) surface: one finds the lower-lying two-fold degenerate sub-bands, corresponding to the in-plane electronic motion with an effective mass $m^* = 0.19m_e$, and four-fold degenerate upper sub-bands with the in-plane effective mass $m^* = 0.916m_e$ [1, p.443]. At the lowest temperatures (and in the absence of a magnetic field) the electrons are believed to populate the lowest of the two-fold

[2]this layer of electrons is called *inversion layer*

degenerate sub-bands.[3]

It was first shown in Ref.[38] that the two-fold valley degeneracy is actually lifted in real Si MOSFET systems. The origin of this splitting is quite controversial [1]. The value of the splitting has been measured, for example, in Ref.[39]: at the electron density $n_s = 2.4 \times 10^{12}\text{cm}^{-2}$ and in a perpendicular field $B_\perp = 4.6\text{T}$, the valley splitting E_v was found to be approximately 0.7meV. It is also known from the measurements in Ref.[40] that E_v increases linearly with increasing depletion charge (which can be varied by the application of a substrate bias – an electric potential between the interface and the bottom surface of Si substrate). Valley splitting can be enhanced by a perpendicular component of the magnetic field [1, p.572], but is not affected by a parallel component [40].

3.2 Measurement technique and experimental challenges.

Almost all the experimental results in Chapter 4 were obtained by 4-terminal transport measurements of samples directly immersed into a ^{3}He–^{4}He mixing chamber (glass tail) of an OXFORD Model 75 Dilution Refrigerator, and positioned at the center of the 9-Tesla superconducting magnet. The angle-dependent magnetotransport measurements of Section 4.4 were performed in an OXFORD HELIOX^{VL} Pumped ^{3}He System[4] equipped with a manual rotator and a 13-Tesla magnet.

The Si MOSFET samples[5] were mounted on 24-pin JADE chip headers. A 0.001″-

[3]which corresponds to the ground state of quantized motion along z direction: $\epsilon(\vec{k}) = \epsilon_n + \hbar^2/(2m)[k_x^2 + k_y^2]$ with $n = 0$.

[4]in A. D. Kent's Laboratory at New York University

[5]obtained from Dr. V. M. Pudalov (Troitsk) and from Prof. R. W. Wheeler (Yale University)

thick aluminum thread was bonded to the sample contact pads[6] using the bonding machine in Prof. A. D. Kent's Laboratory at NYU.

For the sample and thermometer leads from the top of the cryostat down to the still of the dilution refrigerator, 0.002″-thick constantan and 0.005″-thick Cu wires glued with GE varnish into two 18-way strips were used. The strips were thermally anchored at several copper heat sinks along the way down: at the upper flange of the Inner Vacuum Can (which is at helium bath temperature, $T = 4.2$ K), and at the He^4 Pot ($T \approx 1.5$ K). At the still ($T \approx 0.6$ K) each of the constantan (and Cu) leads terminates and connects to 0.012″-thick Nb-Ti (in Cu-Ni alloy cladding)[7] wires that extend down to the top of the mixing chamber. The hermetically sealed feed-through provides a connection of Nb-Ti leads with Cu leads inside the mixing chamber. Finally, the copper leads are soldered to the chip carrier socket posts. This arrangement minimizes heat transfer from room temperature to the still (by careful thermal anchoring), and from the still into the mixing chamber (by introducing leads made of a poor thermal conductor - superconducting filaments in alloy cladding). The large thermal conductivity of copper leads inside the mixing chamber establishes thermal equilibrium along the length of the chamber.

To reduce RF heating, π-filters (that leave the phase of the signal unchanged because of purely imaginary impedance) were attached to the 18-way FISCHER connectors at the top of the cryostat[8].

The temperature was measured by two Dale 1kOhm-series RuO resistors mounted at the top and bottom of the sample chip carrier holder. The temperature was controlled with one of the thermometers (calibrated in a magnetic field) using a BIO-

[6]samples from Dr. Pudalov's supply came fully processed

[7]This choice of superconducting wire was suggested by Prof. Eric Smith at Cornell.

[8]The filters obtained from SPECTRUM CONTROL INC. were connected by Mr. D. Przybylski into a FISCHER-compatible plug-in for the signal lines

MAGNETIC TECHNOLOGIES Bridge Controller; the other thermometer was monitored by a standard 4-terminal method at 13 Hz using a STANFORD RESEARCH SYSTEMS 850 Lockin Amplifier, and a generic calibration was used to monitor the temperature gradient along the length of the sample holder.

Contacts to the inversion layer in a Si MOSFET at *low* electron densities (*i. e.* on the order of 10^{11} cm^{-2}) at temperatures characteristically below 1.5 K become capacitive and diodic. This circumstance makes the ac 4-terminal method difficult, due to uncontrolled reactive components. All the low-temperature measurements in Chapter 4 were performed using dc. Resistivities were deduced from the dc IV characteristics, measured for each electron density set by the gate voltage V_g. The "symmetric" variation of the 4-terminal measurement setup suggested by Dr. Pudalov was homebuilt and is shown in Figure 3.2. The current source is completely disconnected from ground (leakage resistance of BURR-BROWN ISO 120 Isolation amplifier is greater than 10^{14} Ohm). The center lead of the sample is grounded; V+ and V− leads are floating (see Figure 3.3). It was verified during the course of measurements that this method is more reliable, and provides much cleaner readings at low n_s and low T than the conventional 4-terminal method in which one of the voltage leads is grounded.

At $T \geq 1.5$ K a 4-terminal ac method at 13 Hz was employed for resistivity measurements. The standard setup used commercially available devices: STANFORD RESEARCH SR 850 Lockin Amplifier at 13 Hz, and VALHALLA SCIENTIFIC Current Calibrator, capable of producing ac currents as low as 1 μA per 1 V of reference signal of SR 850.

3.3 Characterization of MOSFET samples.

Experimentally measured parameters of the system that are essential to us are the density of carriers in the 2D layer n_s, and the electron mobility μ, which is a function of n_s. For the rest of this work, the mobility will be determined from the Equation 2.11:

$$\mu(n_s) = (\rho_{xx}(n_s)en_s)^{-1}; [\mu] = \text{cm}^2/(\text{Vs}). \tag{3.2}$$

Here $\rho_{xx}(n_s)$ is the longitudinal resistivity in ohms, electron charge $e \equiv 1.6 \times 10^{-19}$ C, and n_s is the electron density in the inversion layer in cm^{-2}. This formula can be easily derived by noting that μ is usually defined as the coefficient of proportionality between the electron drift velocity and the electric field, and making use of the Drude conductivity form, $\sigma = e^2\tau n_s/m^*$. The use of Drude's form implies that Eq. 3.2 is only meaningful when the Ioffe-Regel condition, $l \gg \lambda_F$, is met. Peak mobility $\mu^{max} \equiv max(\mu(n_s))$ at 4.2 K can be thought of as a measure of the disorder that electrons in the inversion layer "see". We refer to peak mobility, which occurs at comparatively high electron densities, where the condition $l \gg \lambda_F$ holds and the form of Eq. 3.2 is applicable. The higher energy sub-bands are already depopulated at 4.2 K and do not contribute to the conductivity, and the phonon scattering is weak [1]. At the same time, the quantum effects, discussed in Section 2.1 on page 4, are not yet dominant. The temperature dependence of the *peak* mobility near 4.2 K is rather weak, which means that it largely reflects temperature-independent electron scattering with imperfections. Of these, scattering off positive charges trapped in the oxide of the MOS system is believed to limit the peak electron mobility at low temperatures [1].

The carrier density of the samples was extracted from Shubnikov-de Haas minima (Quantum Hall minima at higher H) of the longitudinal resistivity ρ_{xx} in a perpendicular magnetic field H. The method is quite straightforward and is essentially similar to the one outlined in Ref.[1, p.490]. ρ_{xx} has a minimum whenever ν levels are filled.

The Fermi level ϵ_F is then midway between the centers of the ν-th and the $(\nu+1)$-th Landau levels, where no extended states are present (see, for example, Ref.[4]). At low enough temperatures this means that no resistive current can flow, hence, $\rho_{xx} \rightarrow 0$[9]. Thus, the longitudinal resistivity minima occur if

$$n_s \equiv k(V_g - V_T) = \nu v, \tag{3.3}$$

where $v \equiv eB/hc$ is the orbital degeneracy, or the number of quantum states in a level per unit of area; c is the speed of light. An example of this analysis is given in Figures 3.4 and 3.3. Even if the spin and valley minima are not resolved, Shubnikov-de Haas oscillations of resistivity in a changing magnetic field on the one hand, and of changing gate voltage on the other hand, allow the determination of both V_T and k. The analysis is easier in higher-mobility samples, since spin levels (and possibly valleys) are resolved, in which case finding the right values for the filling factors corresponding to the minima is very straightforward, and may not require both H– and V_g– sweeps.

Once the electron density has been determined as a function of gate potential, the determination of peak sample mobility is straightforward. The zero-field resistivity is then measured as a function of V_g. The electron mobility is then calculated using Equation 3.2, and plotted versus n_s. The characteristics of the samples used to obtain the results of the next Chapter are summarized in the Table 3.3 below.

[9]The somewhat counterintuitive fact is that in such a case, $\sigma_{xx} \equiv \frac{\rho_{xx}}{\rho_{xx}^2+\rho_{xy}^2} = \frac{0}{0+number^2} = 0$.

Sample number	Nominal oxide thickness ($\AA$)	$\mu^{max}_{T=4.2\ K}$ ($\times 10^4$ cm^2/Vs)	$n_s(V_g)$ (cm^{-2})
P1	2000	2.5	$1.1 \cdot (V_g - 0.6\text{V})$
P2	2000	2.4	$1.1 \cdot (V_g - 0.49\text{V})$
P3	2000	1.7	$1.1 \cdot (V_g - 0.01\text{V})$
W01	600	0.8	$3.47 \cdot (V_g - 0.06 \pm 0.003\text{V})$

Table 3.1: Characteristic of the MOSFET samples: peak mobility μ^{max} and dependence of electron density n_s on the gate potential.

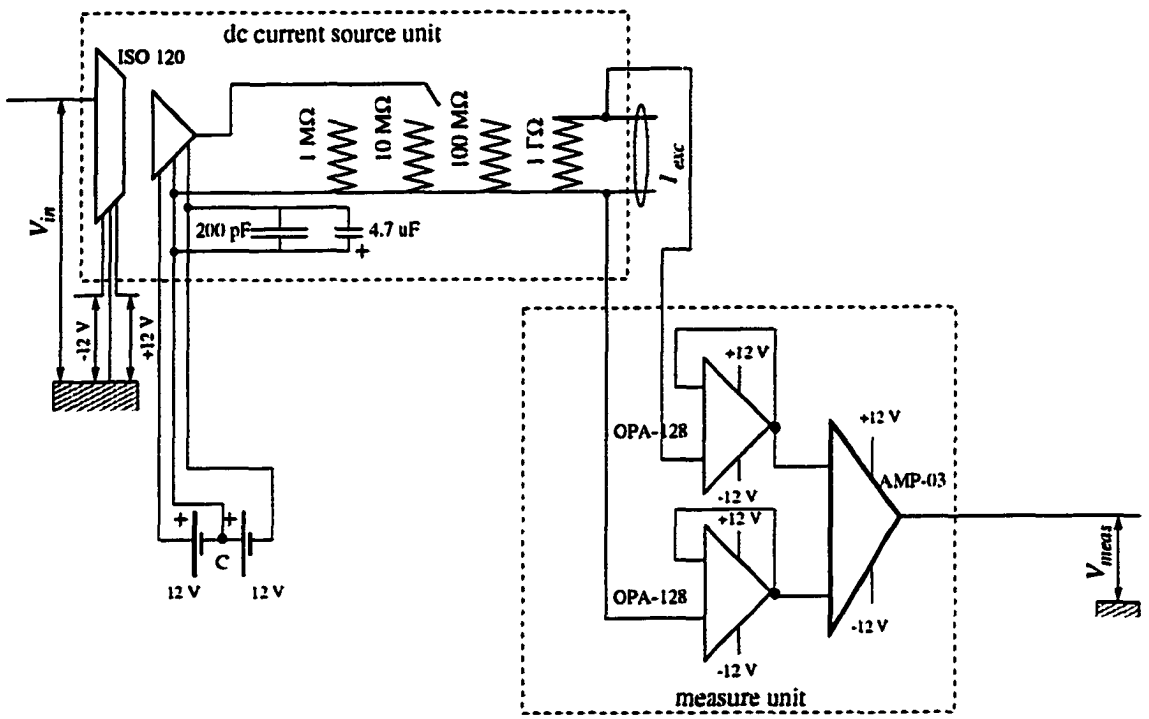

Figure 3.2: A dc input voltage V_{in} is supplied to the home-built Source Unit by KEITHLEY dc source 236. The output of ISO 120 is completely disconnected from ground and equal to V_{in} (relative to point C of the battery source). The range switch allows for sample excitation currents I_{exc} as low as 10 pA. The Measure Unit picks up the voltage drop across the range-setting resistor R_r, so that $I_{exc} = V_{meas}/R_r$. The difference of two electrometer-grade BURR-BROWN OPA 128 readings is read by the ANALOG DEVICES AMP-03 differential amplifier.

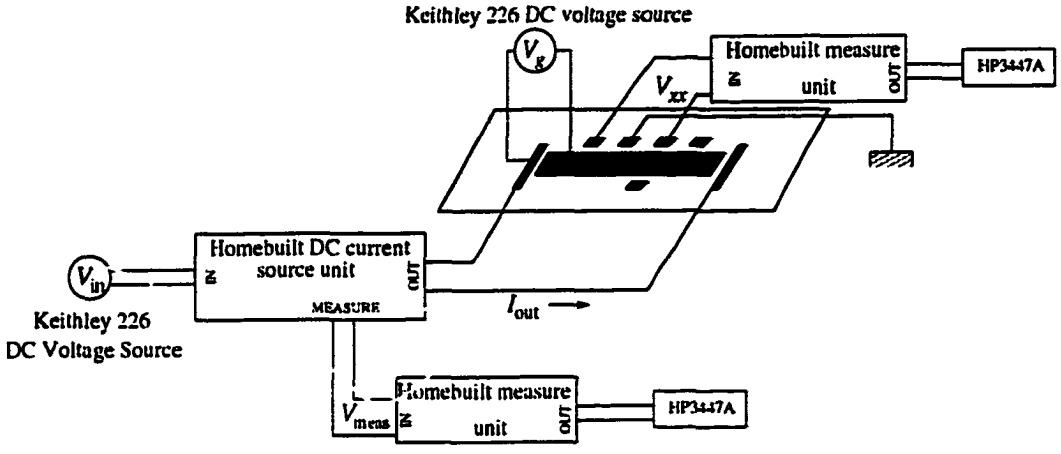

Figure 3.3: Stepwise input voltage V_{in} in the range $-V_0 < V_{in} < V_0$, is supplied to the home-built Source Unit by KEITHLEY dc voltage source 236 controlled by LABVIEW program. The range switch of the Source Unit chooses the dc excitation current range (10 pA to 1 μA). The output $V_{meas} = I_{exc}R_r$ of the homebuilt measure unit shown in the lower part of Figure 3.2 on page 32 is read by the HP voltmeter at every value of V_{in}, thereby monitoring the actual output current I_{exc}. Another measure unit (identical to the one shown in the lower part of Figure 3.2) monitors the voltage drop on the sample.

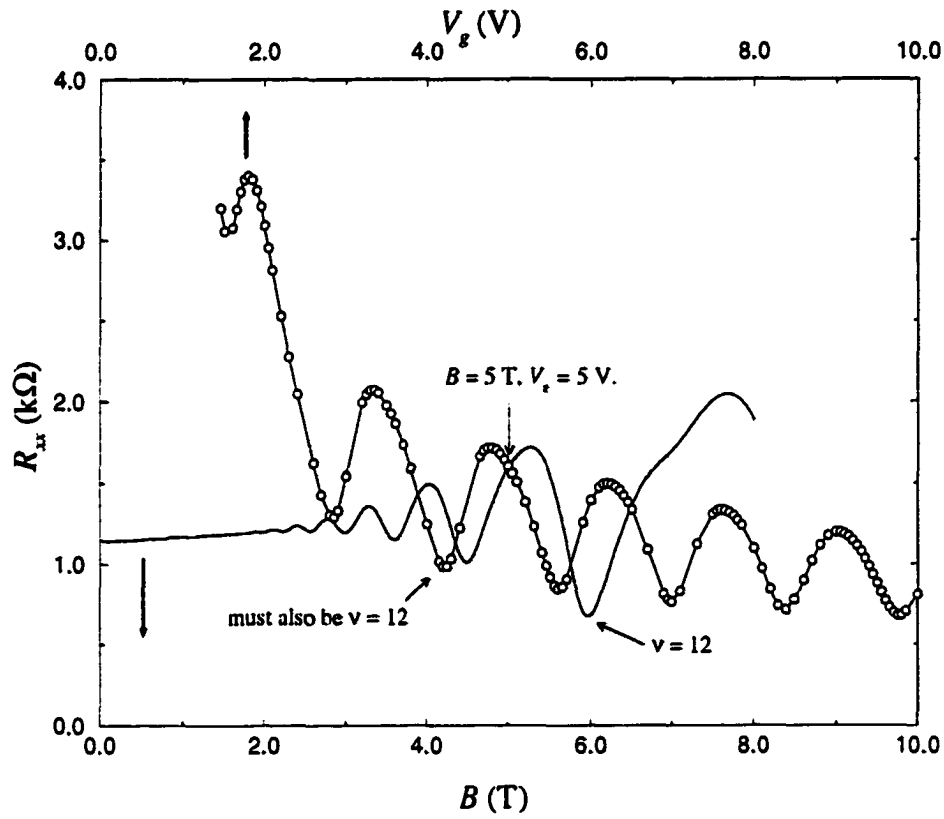

Figure 3.4: An example of sample characterization. The longitudinal resistivity of a low-mobility sample ($\mu_{4.2K}^{max} \approx 8,000$ cm^2/Vs) was measured at $V_g = 5$ V as a function of a magnetic field (solid curve, bottom scale of H), and at a fixed $H = 50$ kOe as a function of gate voltage (opaque circles, top scale of V_g). The positions of the resistivity minima must be proportional to $1/H$. This condition allows identification (see Figure 3.5) of the minimum at $H = 60$ kOe with $\nu = 12$. Each oscillation of ρ includes 4 levels, since neither spins nor valleys are resolved. (Spin level is becoming vaguely resolved at $H \approx 70$ kOe, as indicated by a "wiggle" in $\rho(H)$ curve at $H \approx 70$ kOe.)

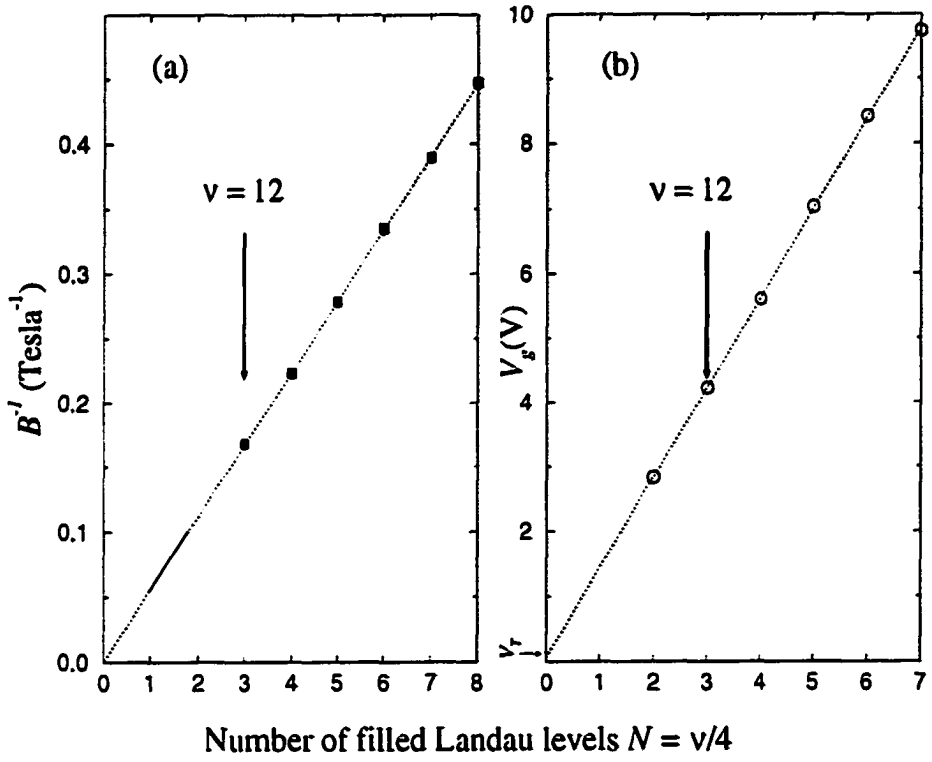

Figure 3.5: (a) Values of B^{-1} corresponding to the resistivity minima (solid curve in Figure 3.4) are plotted *vs* the number of filled Landau levels N. Neither spins or valleys are resolved; each LL contains 4 levels, $N = \nu/4$. Adjacent minima differ by unity in N, the "absolute" values for N are found from the condition that B^{-1} must be proportional to N. This allows identification of the minimum at $H = 60$ kOe with $N = 3$ (or $\nu = 12$). This minimum is the *nearest* to the point ($V_g = 5$V; $H = 50$kOe) on the solid curve in Figure 3.4 (if one moves towards lower filling factors along the curve). Therefore, the nearest minimum to the same point along the V_g–sweep must also correspond to $\nu = 12$. This minimum is indicated by an arrow in plot (b). Fitting to a linear dependence, $V_g - V_T \propto N$, one finally obtains: $n_s[10^{11}\text{cm}^{-2}] = 3.47 \times (V_g - 0.060 \pm 0.003\text{V})$.

Chapter 4

EXPERIMENTAL RESULTS

In this Chapter I present several new observations near the $B = 0$ metal-insulator transition in a 2D system in Si MOSFETs:

• Scaling of the resistivity $\rho(\delta_n)$ with electric field and temperature, and experimental determination of the critical exponents z and ν [41].

• Transport symmetry across the transition: $\rho(\delta_n)/\rho_c = \sigma(-\delta_n)/\sigma_c$ [42].

• Suppression of the conducting state by an external magnetic field[43]; H/T scaling of magnetoconductivity [44]; insensitivity of this effect to the angle between magnetic field and the plane of electrons [45].

• By the application of a magnetic field parallel to the plane of 2D system, restoration of the "ordinary" properties exhibited, for example, by strongly disordered GaAs/AlGaAs [45].

4.1 Scaling of the Resistivity with Electric Field.

The original measurements of S. V. Kravchenko and his coworkers[6, 25, 46] (reviewed in Section 2.3 on page 13) have shown clear signatures of a conductor-insulator transition in a high-quality two-dimensional electron system (2DES) in silicon in zero magnetic field. The resistivity, ρ, was found to scale with temperature, so that

$$\rho(T, n_s) = f_1(|\delta_n|/T^b) \text{ with } b = 1/z\nu. \tag{4.1}$$

Here n_s is the electron density. $\delta_n \equiv (n_s - n_c)/n_c$, n_c is the critical electron density at the metal-insulator transition. z is the dynamical exponent, and ν is the correlation length exponent introduced in Section 2.4 on page 18. The resistivities reported in Refs. [6, 25] were obtained in the linear regime, *i.e.*, in the limit of zero electric field, $E \to 0$. When the electric field is strong, however, the effective temperature of the electrons becomes higher than that of the lattice. Scaling analysis, reviewed in Section 2.4, shows that the resistivity should also scale with the electric field, but the scaling exponent in this case will be $1/[(z+1)\nu]$ (instead of $1/z\nu$ in the case of temperature scaling) so that

$$\rho(E, n_s) = f_2(|\delta_n|/E^a) \text{ with } a = 1/[(z+1)\nu]. \tag{4.2}$$

Knowing both $z\nu$ and $(z+1)\nu$ is sufficient to determine the exponents z and ν separately.

The resistivity of samples with maximum electron mobility $\mu_{4.2\,K}^{max} \approx 17 - 24{,}000$ cm^2/Vs was determined as a function of electric field by measuring current versus voltage (IV curves) for many values of n_s using a four-terminal dc technique outlined in Section 3.2 on page 26. Typical curves are shown in Figure 4.1. The middle, solid curve — approximately a straight line — separates all IV curves into two groups exhibiting different types of nonlinear behavior. The S–shape, corresponding to lower electron densities, is associated with insulating behavior. One can notice by looking

at any of the S-shaped curves in Figure 4.1 that the *slope* of the line connecting the origin to a point on a curve (which is the sample resistance) decreases with the increasing current (which determines the effective electron *temperature*). Thus, the resistivity decreases with increasing temperature, which is characteristic of an insulator. Similar arguments can be made to associate Z-shape, corresponding to higher electron densities, with metallic behavior. The middle straight line signals current-independent resistivity, and should, therefore, be identified with the critical curve (for which $n_s = n_c$).

Quite a remarkable symmetry about the middle curve can be noticed in Figure 4.1. This symmetry and its implications will be considered in detail in Chapter 5 on page 74. A straightforward algebraic transformation of the experimentally measured $V(I)$ dependences yield the curves of resistivity ρ *vs* electric field E for different electron densities that are shown in Figure 4.2 (not all curves measured are shown in order to avoid too high a density of points). Here, the resistivity is determined from $\rho = (V/I) \cdot (W/L)$ (W is the sample width and L is the distance between potential contacts) and the electric field $E = V/L$. Again, there is clearly a critical electron density which separates two distinct density regions characterized by different types of resistivity behavior as a function of electric field. At the critical point, the resistivity (solid curve in Figure 4.1, closed circles in Figure 4.2) is virtually independent of the electric field and close to $3h/e^2$. All curves below this line are characterized by $d\rho/dE > 0$ while all curves above are characterized by $d\rho/dE < 0$. The observed critical behavior of ρ as a function of E is very similar to the critical behavior of the resistivity with *temperature* observed near the conductor-insulator transition in 2DES in silicon [6, 25][1] It also resembles the behavior found near the superconductor-insulator phase transition in thin metallic films [29] and the quantum Hall effect-

[1] with the only difference that the resistivity at the critical point is E-independent for the measured range of E, but not T-independent at $T > 2$ K.

insulator (QHE-I) transition in GaAs/AlGaAs heterostructures [47, 48, 49].

A remarkable property is that plotting the resistivity against the scaling variable, $|\delta_n|/E^a$, causes all the curves to collapse onto two distinct branches, as shown in Figure 4.3. Note that points for $E \to 0$, where ρ saturates due to finite temperature of the lattice, have been omitted.[2] As expected, the scaling fails at electron densities far from the critical point where the system is no longer in the critical regime, as seen on the lower (metallic) branch in Figure 4.3. The upper branch corresponds to $n_s < n_c$ and the lower one to $n_s > n_c$. At the transition ($n_s = n_c$), the resistivity is close to $3h/e^2$. It is interesting to note that almost the same value was observed in Ref. [50] for a transition between weak and strong localization in disordered metallic films. The exponent a was varied to obtain the best visual collapse, yielding $a = 0.37 \pm 0.01$.

4.2 Determination of the Correlation Length and Dynamical Exponents.

Reproducing the measurements reported in Refs. [6, 25], the temperature dependences of the resistivity of the same Si MOSFET sample (as in Section 4.1) in the linear regime ($E \to 0$) was measured in the temperature range 0.22 K< T <1 K in the mixing chamber of the dilution refrigerator using the technique outlined in Section 3.2. Resistivity curves for different electron densities are shown in Figure 2.3. These data were used to obtain scaled curves of the resistivity as a function of the *temperature*-dependent scaling variable, $|\delta_n|/T^b$. This is shown in Figure 4.4, where it is evident that all curves again collapse onto two distinct branches, confirming the earlier results of Kravchenko *et al.* reviewed in Section 2.3 on page 13. We note that the data scale

[2] so small an electric field is that it no longer determines the effective temperature of electrons.

well only at temperatures below 1 K, presumably because at higher temperatures the system is outside the critical regime. The best collapse was achieved for $b = 0.83 \pm 0.08$. As was mentioned in Section 4.1, electric field– and temperature–scaling analyses performed on the same sample, allow one to determine both the dynamical exponent and the correlation length exponent. Indeed, from

$$\begin{cases} b = 1/z\nu = 0.83 \\ a = 1/[(z+1)\nu] = 0.37, \end{cases} \tag{4.3}$$

one derives: $\nu = 1.5 \pm 0.1$ and $z = 0.8 \pm 0.1$. While the correlation length exponent has not been theoretically predicted for this system, the value of the dynamical exponent in a strongly interacting 2D system was predicted to be $z = 1$ [26], fairly close to what we observe. In the majority of interacting 2D systems where it has been determined, the exponent z has also been found to be close to 1 (see, *e.g.*, Ref. [28] for the case of a superconductor-insulator transition and Ref. [37] for the transition between two neighboring QHE plateaus). The same result for the case of hopping conductance (on the insulating side of the transition) follows from the theory of Polyakov and Shklovskii [51] who found the ratio of scaling exponents $a/b = 1/2$ (see Equations 4.1 and 4.2) which is equivalent to $z = 1$.

The significance of the electric-field scaling analysis in which we assumed the behavior near the quantum critical point is discussed and compared with the alternative picture of phonon heating in Chapter 5.

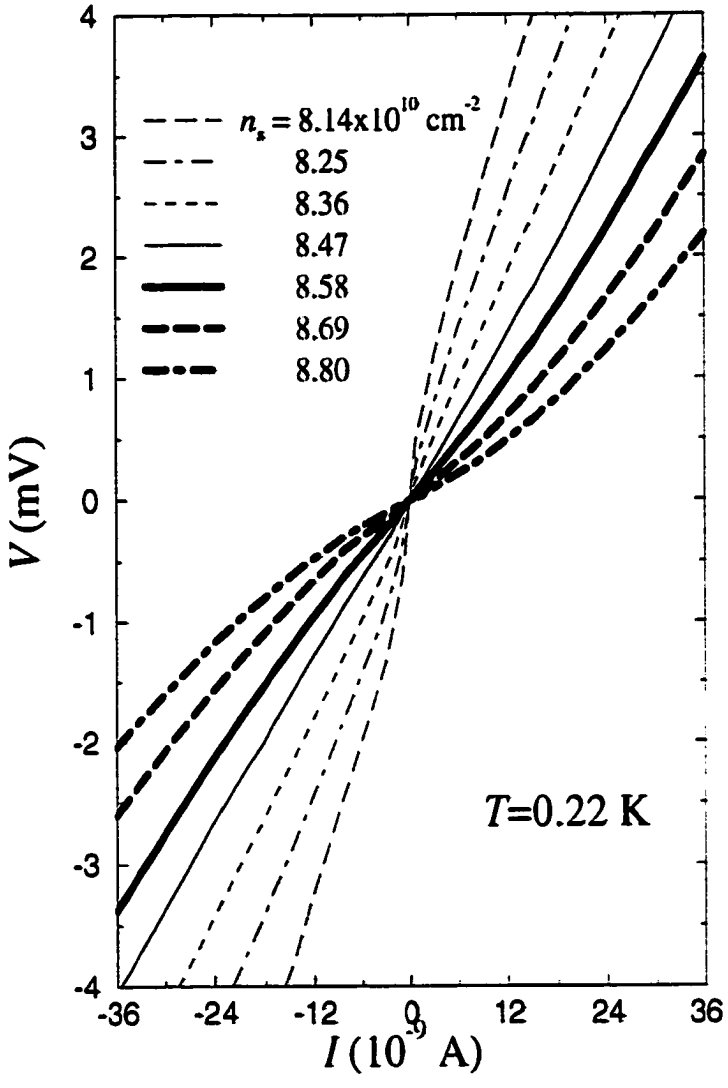

Figure 4.1: Nonlinear current-voltage curves at several electron densities around the metal-insulator transition. $T = 0.22$ K.

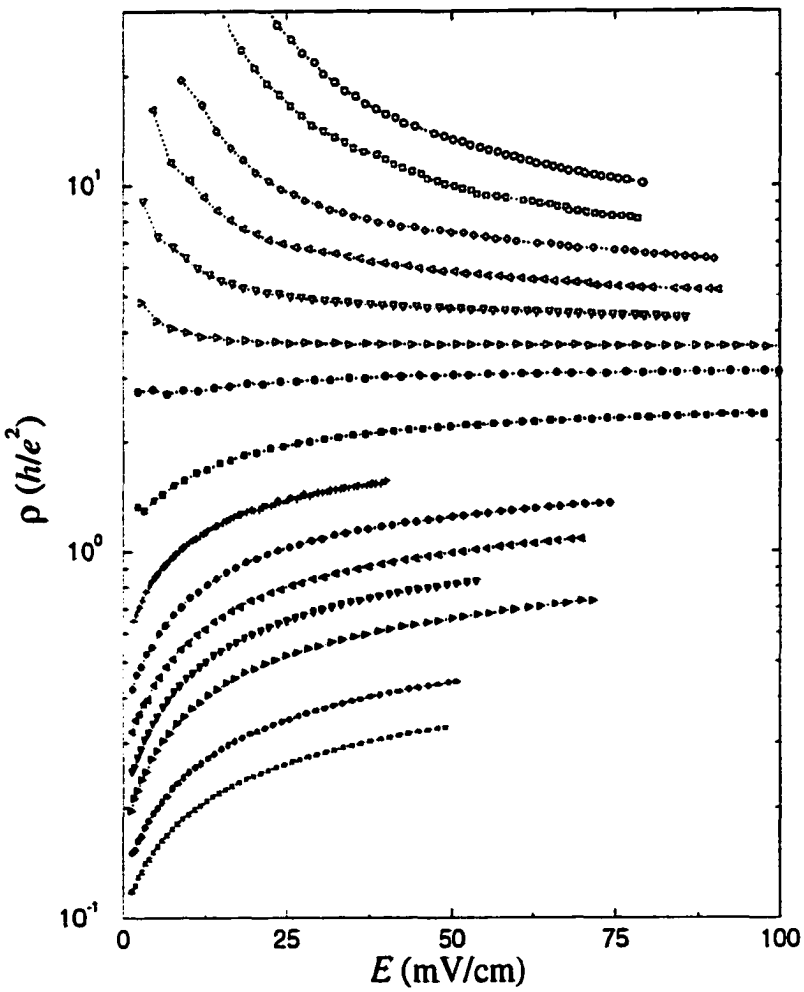

Figure 4.2: Resistivity as a function of electric field at n_s = 7.81, 7.92, 8.03, 8.14, 8.25, 8.36, 8.47, 8.70, 8.91, 9.13, 9.35, 9.57, 9.79, 10.34, and 10.78 × 10^{10} cm^{-2} at $T = 0.22$ K.

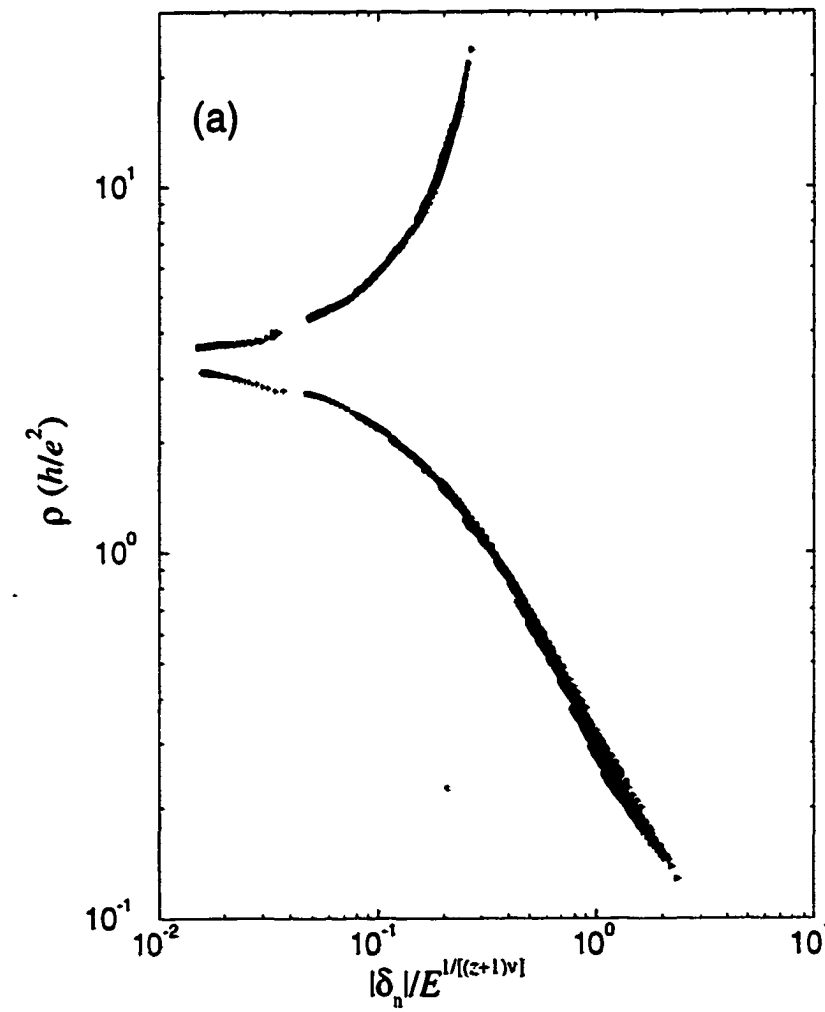

Figure 4.3: Demonstrating scaling with electric field, the resistivity in the non-linear regime at 0.22 K is plotted as a function of $|\delta_n|/E^a$ for $a = 1/[(z+1)\nu] = 0.37$.

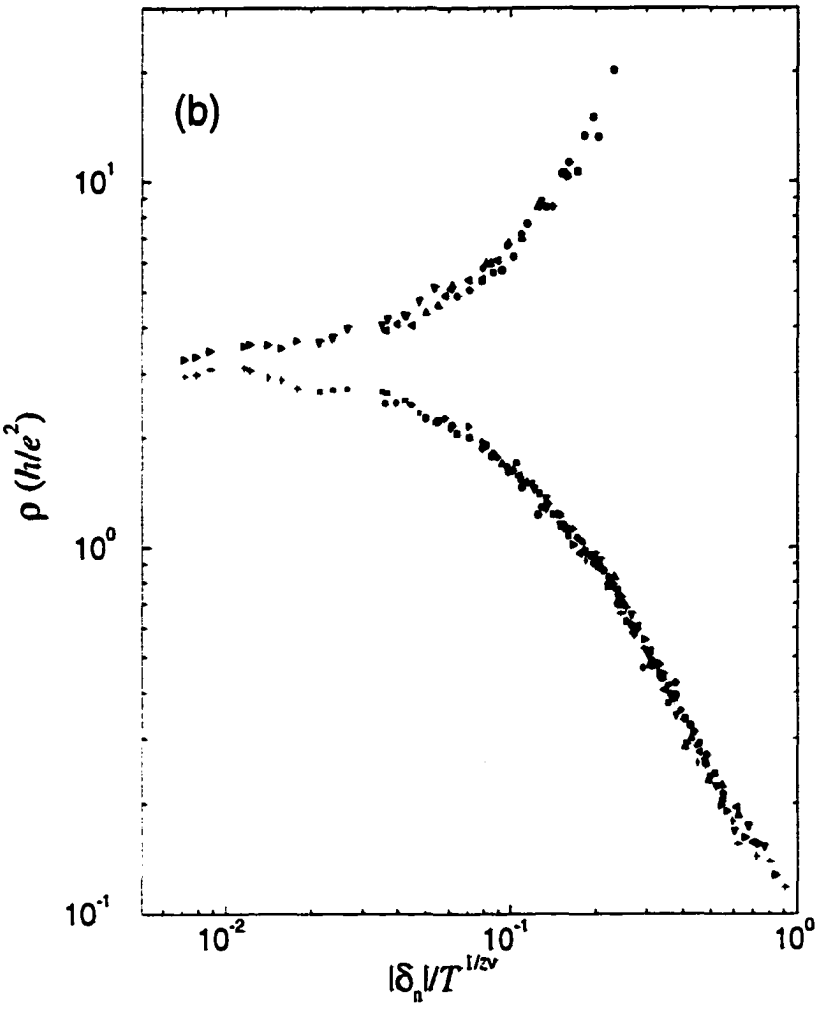

Figure 4.4: Demonstrating scaling with temperature, the linear resistivity ($E \to 0$) is shown as a function of $|\delta_n|/T^b$ for $b = 1/z\nu = 0.83$. Electron densities are in the range 7.81 to 10.78 $\times$ 10^{10} cm^{-2}.

4.3 Symmetry of the Resistivity and Conductivity Across the Transition.

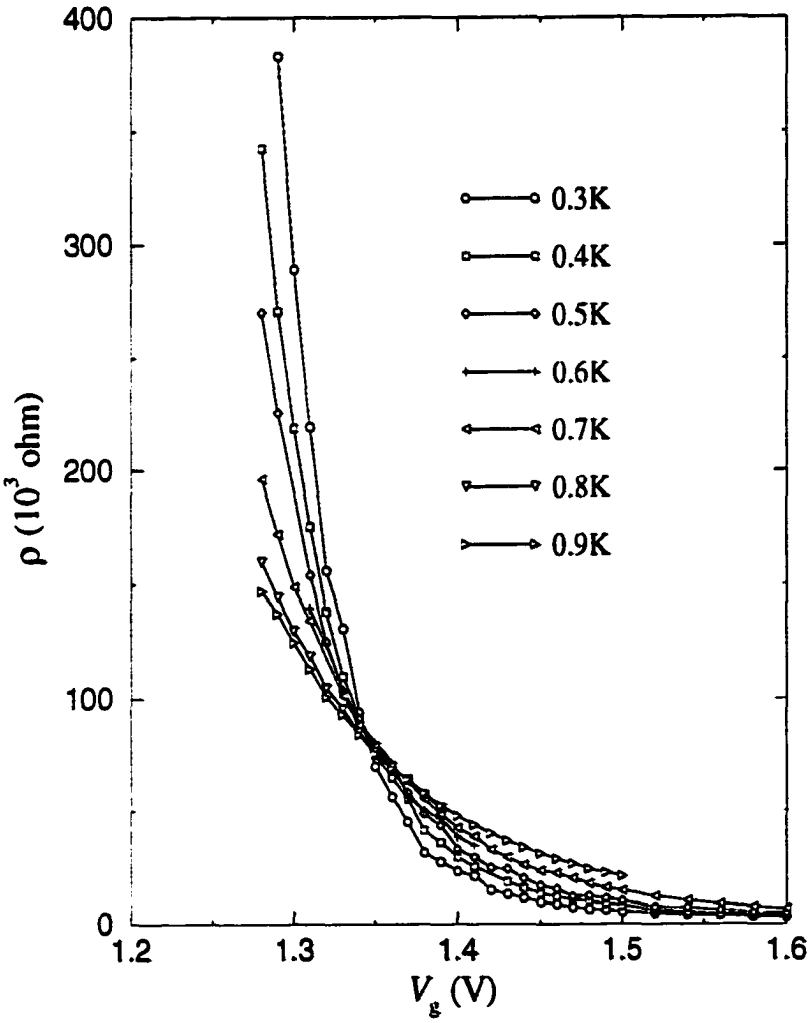

Figure 4.5: Resistivity as a function of gate voltage, V_g, for temperatures between 0.3 K and 0.9 K, obtained from the linear portion of the IV curves using the appropriate dimensionless geometric factor.

A remarkable property of the temperature-dependent resistivity in the linear regime near the MIT will now be deduced empirically from the data in Figure 2.3 on

page 17. The following recent observation has prompted this analysis. In GaAs/AlGaAs heterostructures, Shahar *et al.* [52] have found a simple relation between the longitudinal resistivity in the magnetic field-induced insulating phase and the neighboring quantum Hall liquid (QHL) phase: $\rho_{xx}(\Delta\nu) = 1/\rho_{xx}(-\Delta\nu)$. Here $\Delta\nu = \nu - \nu_c$, and ν_c is the critical filling factor for the $\nu = 1$ QHL-insulator transition; the relation also holds for the fractional $\nu = 1/3$ QHL-insulator transition when mapped [53] onto the $\nu = 1$ QHL-insulator transition of composite fermions. Shahar *et al.* [52] point out that this remarkable symmetry indicates a close relation between the conduction mechanisms in the two phases.

A similar symmetry near the critical electron density for the $B = 0$ metal-insulator transition in the 2D electron gas in high mobility silicon MOSFETs can be argued as follows. Figure 4.5 shows the resistivity as a function of gate voltage (electron density) at several different temperatures between 0.3 K and 0.9 K. The curves all intersect at a single value of the gate voltage, $V_g = 1.348$ V, corresponding to a critical electron density, $n_c = 8.45 \times 10^{10}$ cm^{-2}. The resistivity decreases (increases) with increasing temperature for $n_s < n_c$ ($n_s > n_c$), as expected for insulating (metallic) behavior. In agreement with earlier measurements[25, 46], the resistivity at the critical point is close to $3h/e^2$.[3]

Now let us normalize the resistivity by its value at the critical density, $\rho_c \approx 3h/e^2$. The normalized resistivity $\rho^*(V_g) \equiv \rho(V_g)/\rho_c$ and the normalized conductivity $\sigma^*(V_g) \equiv \sigma(V_g)/\sigma_c$ at $T = 0.35$ K are shown as functions of the gate voltage in Fig. 4.6. Note the apparent symmetry about the vertical line corresponding to the critical electron density.

Fig. 4.7 demonstrates that the curves can be mapped onto each other by reflection, *i.e.*, $\rho^*(\delta_n)$ is virtually identical to $\sigma^*(-\delta_n)$. Data indicate that this mapping holds

[3]Note that existence of a single crossing point at n_c is a consequence of a temperature-independent (between 0.3 K and 0.9 K) separatrix $\rho(n_s = n_c) \equiv 3h/e^2$.

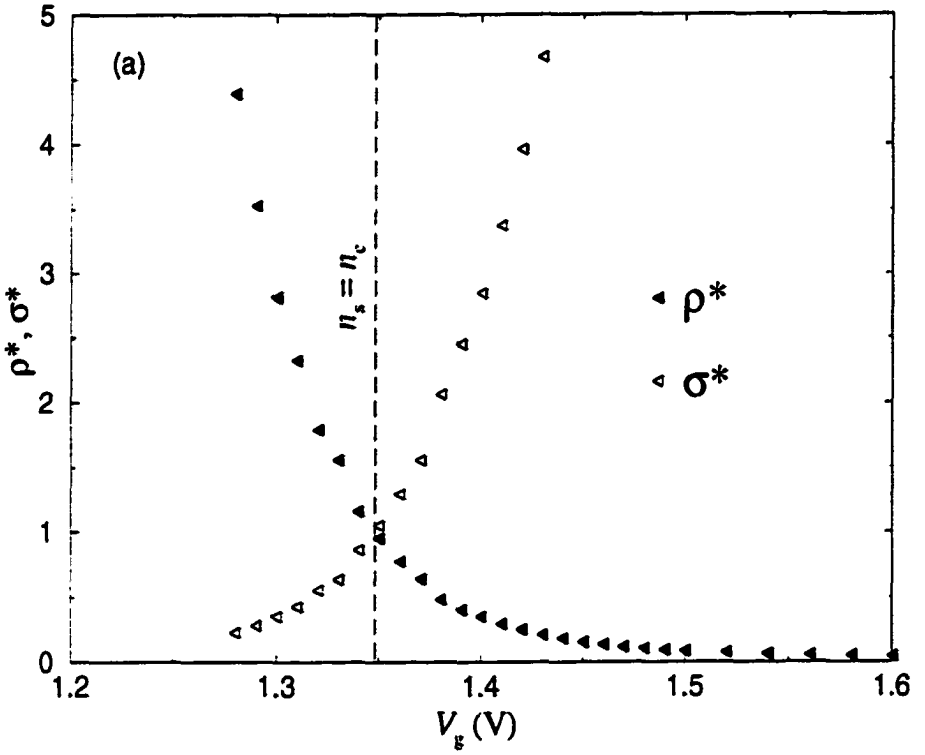

Figure 4.6: Normalized resistivity, ρ^*, and normalized conductivity, σ^*, as functions of the gate voltage, V_g, at $T = 0.35$ K. Note the symmetry about the line $n_s = n_c$. The electron density is given by $n_s = (V_g - 0.58\text{V}) \times 1.1 \times 10^{11}$ cm^{-2}.

over a range of temperature from 0.3 K to 0.9 K. The range $|\delta_n|$ over which it holds decreases continuously as the temperature is decreased: for example, at $T = 0.9$ K, ρ^* and σ^* are symmetric for $|\delta_n| < 0.1$, while at $T = 0.3$ K, they are symmetric only for $|\delta_n| < 0.05$ (see inset to Fig. 4.7). On the other hand, the range of resistivity for which the mapping is valid remains approximately unchanged with temperature. Thus, over a range of temperature 0.3 K $\leq T \leq$ 1 K, the (normalized) linear conductivity on either side of the transition is equal to its inverse on the other side:

$$\rho^*(\delta_n, T) = \sigma^*(-\delta_n, T). \tag{4.4}$$

The implications of this symmetry will be discussed in Chapter 5.

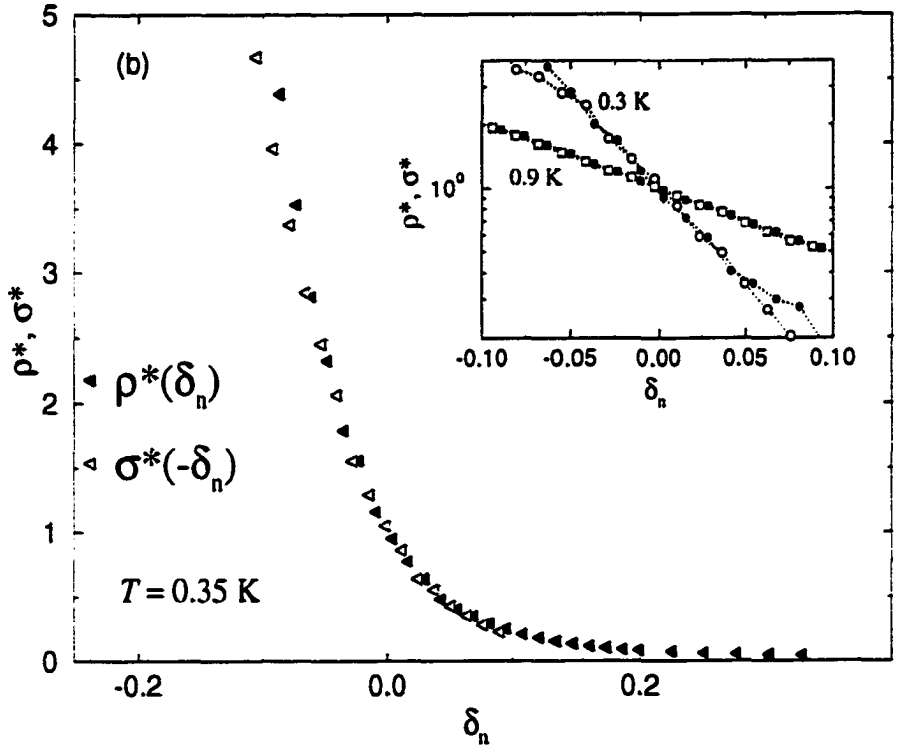

Figure 4.7: To demonstrate this symmetry explicitly, $\rho^*(\delta_n)$ (closed symbols) and $\sigma^*(-\delta_n)$ (open symbols) are plotted versus $\delta_n \equiv (n_s - n_c)/n_c$. Inset: $\rho^*(\delta_n)$ (closed symbols) and $\sigma^*(-\delta_n)$ (open symbols) versus δ_n at $T = 0.3$ K and $T = 0.9$ K, the lowest and highest measured temperatures.

4.4 Suppression of the Conducting State by an External In-Plane Magnetic Field

So far we have learned that the transition occurring in the absence of a magnetic field in high-mobility, low-density MOS devices exhibits scaling behavior (expected of a quantum phase transition) with temperature [6, 25] and with electric field [41]. It has been also shown [42] that linear resistivity near the critical density possesses the transport symmetry expressed formally in Equation 4.4 on page 47. The mechanism of this transition is not understood. In this Section, I show that electrons' spins are central to the appearance of the anomalous conducting phase. Measurements of the resistivity in a magnetic field applied parallel to the plane of electrons at temperatures and carrier densities where the $H = 0$ conducting phase exists indicate that a *parallel* magnetic field has a dramatic effect on the transition, entirely eliminating the conduction mechanism responsible for the existence of the $H = 0$ conducting phase above $\sim$ 20 kOe. An in-plane magnetic field couples to the spins, but not to the orbital motion, thereby allowing us to study the influence of strong magnetic fields without entering the quantum Hall regime[4].

The results of measurements of the linear and nonlinear DC resistivities of high-mobility Si MOSFET samples P2 and P3 are presented below; data for other high-mobility samples gave similar results. Let us recall that equivalent information is obtained from the temperature-dependence of the linear resistivity (in the limit $E \rightarrow 0$) and the electric-field-dependence of the nonlinear resistivity in the limit $T \rightarrow 0$, as was demonstrated in Section 4.1 on page 37 by similar behavior near the critical point in the two cases. Measurements as a function of electric field are easier to perform and entail smaller errors. The resistivity was measured as a function of parallel

[4]where the electronic transport is determined by the perpendicular component of a field $H_\perp$, and does not tell about the $H = 0$ phase.

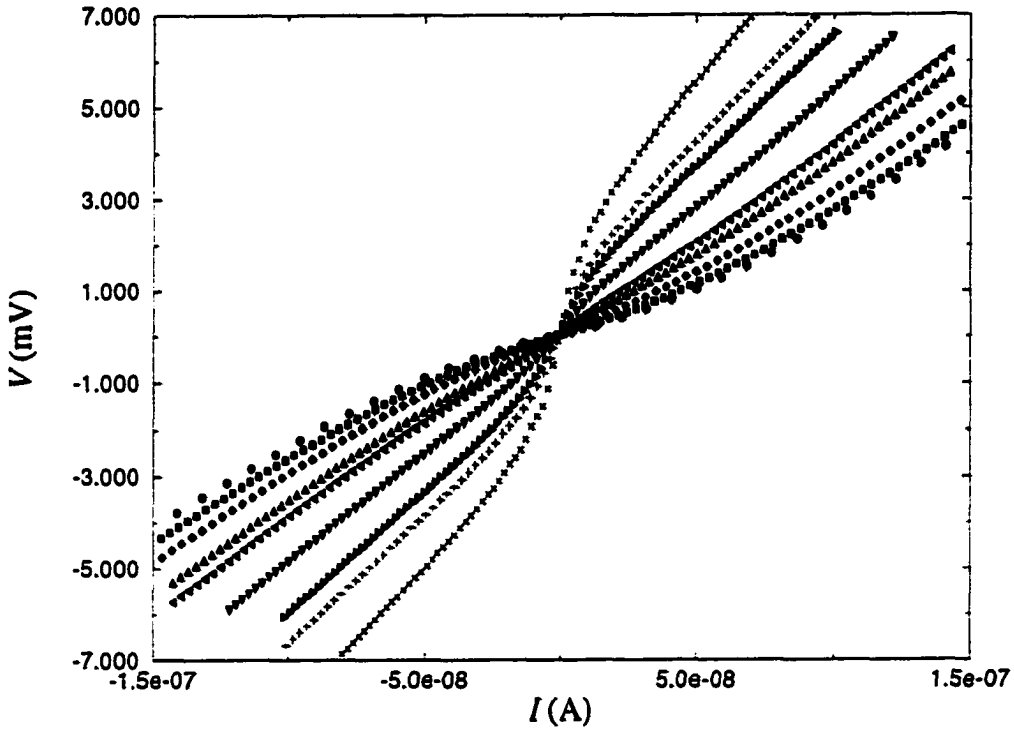

Figure 4.8: IV curves for a fixed electron density in a changing in-plane magnetic field. V_g = 0.82 V, which corresponds to electron density $n_s = 9.02 \times 10^{10}$ cm^{-2}. At $H = 0$ (circles) the sample is on the conducting side of the MIT. The localizing effect of an in-plane field is obvious from the gradual change of the shapes of IVs as the field is increased. H changes from 4kOe (squares) to 16 kOe (crosses).

magnetic field, at various temperatures, and for different values of the electric field (determined by the measuring current). No difference was found for *in-plane* magnetic fields applied parallel and perpendicular to the measuring *current*.

In Section 4.1 we were able to identify metallic and insulating behavior of a sample by examining characteristic shapes of the IV curves shown for the $H = 0$ case in Figure 4.1 on page 41. It follows from that discussion that by decreasing electron

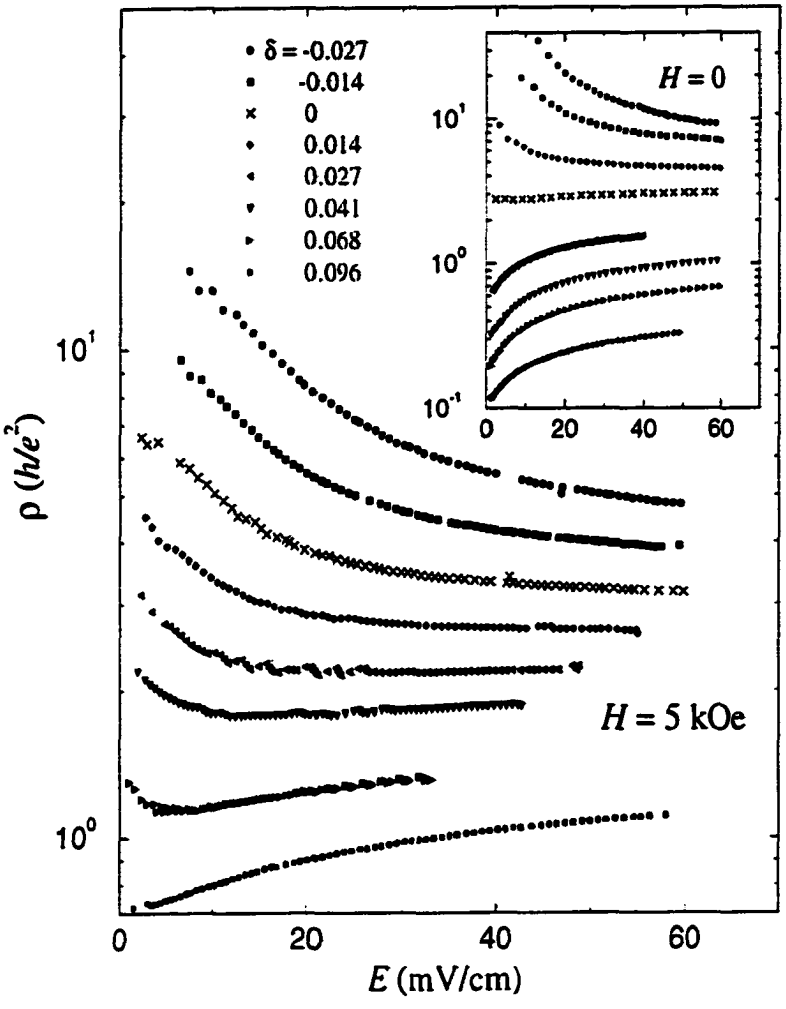

Figure 4.9: Resistivity as a function of electric field on a semilogarithmic scale at $H_{||} = 5$ kOe and $T = 0.10$ K. Electron densities are specified relative to the $H = 0$ critical density, $n_c = 8.03 \times 10^{10}$ cm^{-2}; $\delta \equiv (n_s - n_c)/n_c$. The inset shows $\rho(E)$ in the absence of a magnetic field at $T = 0.22$ K, for δ=-0.065, -0.050, -0.030, 0, 0.052, 0.10, 0.16, and 0.27. The crosses correspond to $\delta = 0$.

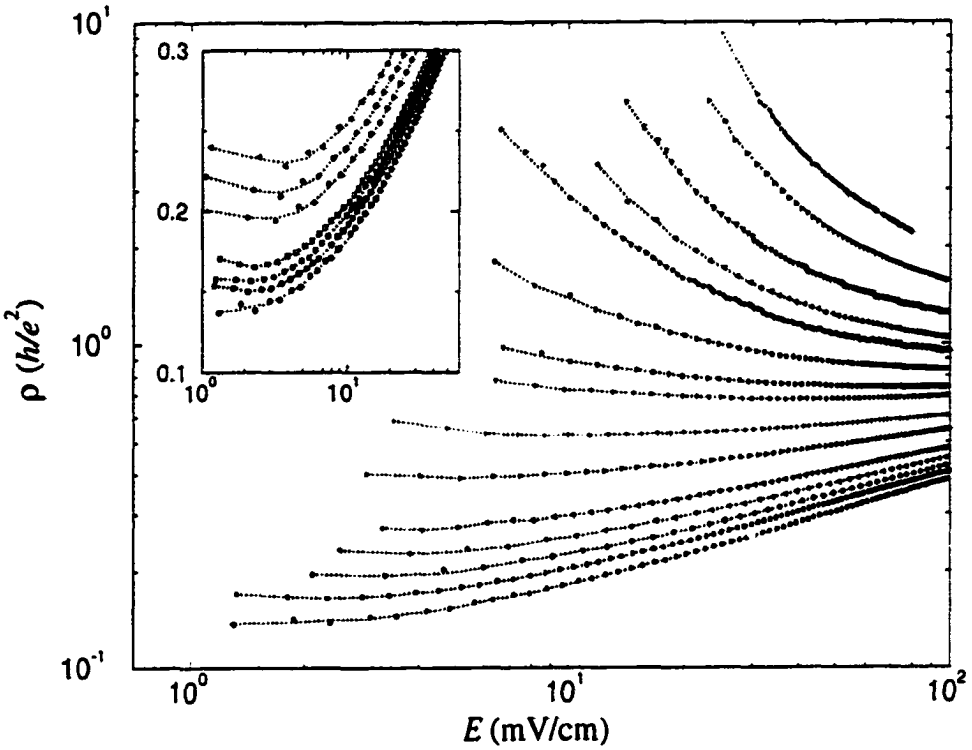

Figure 4.10: Isomagnetic curves of nonlinear resistivity as a function of electric field on a log-log scale for fixed electron density, $\delta_n = 0.3$, at $T = 0.10$ K. Each curve corresponds to a different value of parallel magnetic field, $H_{||} = 0$ (bottom curve), 6, 8, 10, 12, 15, 17, 19, 20, 22, 24, 25, 27, 30, and 34 kOe. Minima in the resistivity are clearly illustrated in the inset, where data are shown on a linear scale for $H_{||} = 0$ (bottom curve), 4, 5, 6, 8, 9, and 10 kOe.

density n_s in the critical region (*i. e.* near n_c) the metallic sample, associated with a Z–shape of its IV curve, can be made insulating, with S–shaped IV.

Now, we measure the IV characteristics of a high-mobility sample with a fixed electron density that places it on the metallic side of the $H = 0$ MIT (corresponding to a zero-field $\delta_n = 0.3$), for different fixed values of parallel magnetic field. The

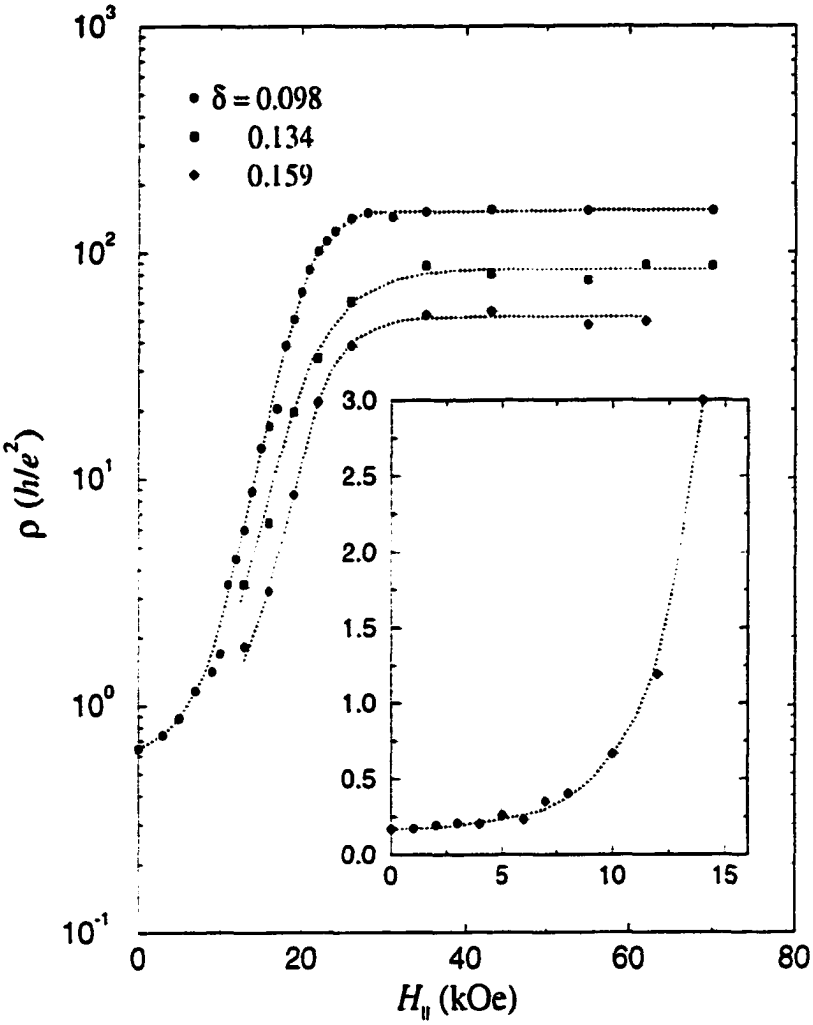

Figure 4.11: Resistivity on a logarithmic scale as a function of a magnetic field applied parallel to the plane at $T = 0.25$ K for three electron densities. The inset shows the resistivity on a linear scale in small magnetic field for $\delta = 0.15$ and $T = 0.13$ K.

temperature of the bath was kept at 0.1 K. These characteristics are shown in Figure 4.8. The immediate significance of this figure is that the sample, metallic at $H = 0$ (Z-shape), can be made quite strongly insulating (S-shape) by a parallel field as low as 10 kOe. At first glance it may seem that the application of an in-plane magnetic field is similar to a decrease in electron density below n_c: both make the

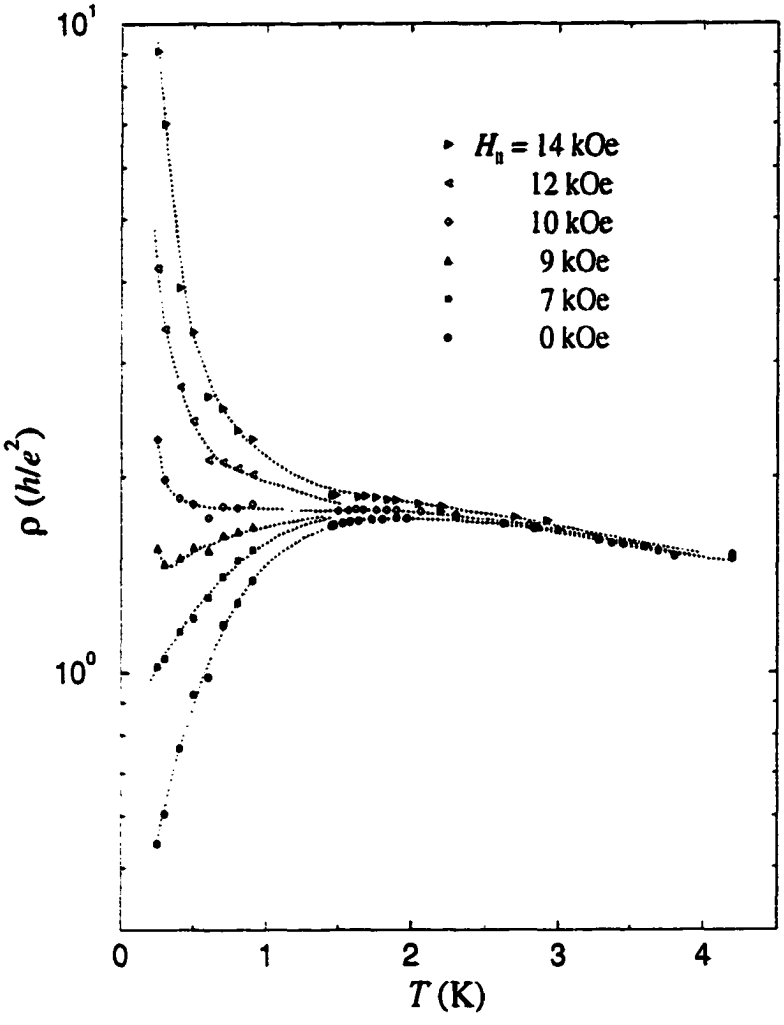

Figure 4.12: Linear resistivity versus temperature in five different parallel magnetic fields. The electron density corresponds to $\delta = 0.10$.

system insulating. However, as it will now become clear, the influence of the parallel field is more dramatic and more complex.

It is sensible to ask at this stage whether one could "compensate" for the insulating effect of a parallel field by increasing the electron density of a MOSFET. In other words, is it possible that the parallel magnetic field simply "shifts" the critical density n_c to a higher value? Figure 4.9 shows the nonlinear resistivity in units of

h/e^2 as a function of electric field in a fixed parallel magnetic field of 5 kOe at a temperature of 0.1 K. The curves in Figure 4.9 are obtained from corresponding IV curves by finding the value of resistivity at each measuring current I. Each curve corresponds to a different electron density (gate voltage). For comparison, the inset shows the resistivity as a function of electric field in the absence of a magnetic field for comparable electron densities. In zero magnetic field, as discussed in Section 4.1 on page 37, the curves clearly separate into two groups: for low electron densities the resistivity increases with decreasing temperature (insulating behavior), while for higher electron densities the resistivity decreases with decreasing temperature (conducting behavior); the resistivity at the transition ($n_s = n_c$) is independent of electric field and approximately equal to $3h/e^2$. As also demonstrated in Section 4.1, a single (horizontal) multiplicative factor can be used to obtain scaling. The effect of a parallel magnetic field is clearly shown in the main part of Figure 4.9: a magnetic field as small as 5 kOe drives all curves toward more insulating behavior. However, there is a qualitative change: for some electron densities the resistivity exhibits non-monotonic behavior, developing a shallow minimum. It is no longer possible to apply a horizontal multiplicative factor to each curve to obtain scaling. It is evident, therefore, that one cannot strictly "compensate" for the insulating effect of a parallel field by increasing the electron density of a MOSFET: the temperature dependences in $H = 0$ and $H \neq 0$ cases are *qualitatively* different.

We now consider whether one can identify a critical parallel magnetic field below which the system is a conductor, and above which it is an insulator. In Fig. 4.10, we plot the nonlinear resistivity, $\rho(E)$, for a fixed electron density (corresponding to a zero-field $\delta = 0.3$) at 0.1 K. Here each curve corresponds to a different value of $H_{||}$. As noted above, the curves are *qualitatively* different from those in zero field shown in the inset to Fig. 4.9: the curves for $\delta > 0$ display a shallow minimum in finite

magnetic field, and it is no longer possible to use a single parameter to collapse them onto two separate branches, insulating and conducting, as was done at $H = 0$ in Section 4.1. Moreover, there is no universal "critical" value of the resistivity, $\rho(H_{||c})$. This suggests that any finite magnetic field (at $T = 0$) drives the system into the insulating phase[5].

The resistivity is shown on a logarithmic scale as a function of magnetic field at a fixed temperature of 0.25 K in Fig. 4.11 for three different electron densities on the conducting side of the $H = 0$ transition ($n_s > n_c$). The resistivity initially changes quite gradually up to $H_{||} \approx 4$ kOe; data at low fields are shown on an expanded scale in the inset to Fig. 4.11 for an electron density corresponding to $\delta \equiv (n_s - n_c)/n_c = 0.15$. The resistivity then increases sharply as the magnetic field is raised further, changing by almost three orders of magnitude. Above $H_{||} \sim 20$ kOe, it saturates and stays approximately constant up to the highest measured field, $H_{||} = 70$ kOe. A parallel magnetic field has dramatically altered the system, apparently suppressing the conduction mechanism in the anomalous conducting phase *entirely* in fields above 20 kOe[6]. The high-field saturation suggests, and it will be shown explicitly in Section 4.6, that above saturation, *i.e.* on having destroyed the $H \to 0$ conduction mechanism, the in-plane magnetic field ceases to affect the system. The behavior is strongly reminiscent of the quenching of superconductivity by a magnetic field (except that the zero-field resistivity in our case is finite rather than zero). The Zeeman energy, $g\mu_B H_{||}$, at 20 kOe corresponds to a thermal energy $k_B T_H$ with $T_H = 2.7$ K. Note that $T_H \sim T^* \approx 2$ K where T^* marks the onset of the low-

[5]I should note, however, that this question is not fully resolved up to date, see Chapter 5 for discussions.

[6]As has been first shown by Pudalov *et al.* [54], the saturation field is a function of electron density n_s. Here we give the characteristic value of H_{sat} in the close proximity to the transition, $\delta_n \approx 0.1$.

temperature conducting phase in zero field (see the $H = 0$ curve in Figure 4.12).

Finally, I show in Figure 4.12 the *linear* resistivity (at $E \to 0$) as a function of temperature for a fixed electron density on the conducting side of the $H = 0$ transition ($\delta = 0.1$) in several parallel magnetic fields between 0 and 14 kOe. The zero-field curve is typical of a conductor, with resistance dropping sharply as the temperature is decreased below ≈ 2 K, while at $H = 14$ kOe it is strongly insulating. The magnetic field has almost *no effect* on the resistivity above $T^* \approx 2$ K, while below T^* the effect of $H_{||}^*$ is enormous (as discussed in the previous paragraph, T^* is the characteristic temperature below which the conducting phase exists in zero field). The presence of non-monotonic behavior of resistivity at intermediate magnetic fields can be noted, although it is not as obvious as for the non-linear resistivity data. Again, one-parameter scaling with temperature breaks down in a parallel field, as did one-parameter scaling with electric field.

The main qualitative conclusion of this Section is that an in-plane magnetic field suppresses the anomalous conducting phase found at $H = 0$ in the 2D electron system in Si MOSFETs. The resistivity increases by several orders of magnitude at low temperatures, saturating above ≈ 20 kOe. The fact that a parallel magnetic field has such a dramatic effect indicates that the electrons' spins play a central role. The fact that the Zeeman energy $g\mu_B H$ and thermal energy $k_B T$ that destroy the conducting phase are roughly comparable further supports this possibility. One-parameter scaling with temperature and electric field, found to hold when $H = 0$, breaks down even in a weak magnetic field, suggesting the elimination of the conducting phase by an arbitrarily small H. More quantitative analysis of the suppression by $H_{||}$ of the $H = 0$ conduction mechanism is presented in the next Section.

4.5 $H_{||}/T$ scaling of magnetoconductance $\Delta\sigma(H_{||}, T)$.

The application of an in-plane magnetic field considered in the previous Section affects the spins of the electrons only, and has no effect on their orbital motion. As I noted above, the quenching of the conducting phase by a magnetic field applied parallel to the plane of the electrons thus provides strong indication that the electrons' spins play a central role in the anomalous conducting phase in these two-dimensional systems. The fact that the Zeeman energy $g\mu_B H$ and thermal energy $k_B T^*$ that suppress the conducting phase are roughly comparable was already mentioned. This led us to explore the possibility that the energy scales of $H_{||}$ and T may be equivalent in determining the magnetotransport, namely, that the magnetoconductance should scale with $H_{||}/T$.[7]

In this Section I show that the positive magnetoconductance of a MOSFET with electron density on the conducting side in the immediate vicinity of the $H = 0$ MIT can indeed be adequately described by the following scaling relation:

$$\Delta\sigma(H_{||}, T) \equiv \sigma(H_{||}, T) - \sigma(0, T) = f(H_{||}/T). \tag{4.5}$$

Here f is an empirically deduced scaling function.

The maximum mobility of the sample P1 used in this experiment was $\mu^{max}_{T=4.2K} \approx$ 25,000 cm^2/Vs). The conductivity was measured in magnetic fields up to 15 kOe applied parallel to the plane of the electrons. Measurements were taken between 0.25 and 0.9 K with the sample immersed in the ^{3}He – ^{4}He mixing chamber of a dilution refrigerator. The electron density was set by the gate voltage at $n_s = 9.43 \times 10^{10}$cm^{-2}, placing the sample on the conducting side and near the conductor-to-insulator transition ($n_c = 8.57 \times 10^{10}$cm^{-2}). In the absence of a magnetic field, the

[7] I am grateful to Lenny Tevlin for suggesting the one-parameter scaling form of $\Delta\sigma(H_{||}, T)$ in two dimensions derived by Lee and Ramakrishnan [55] for a disordered (albeit *weakly* interacting) electron gas.

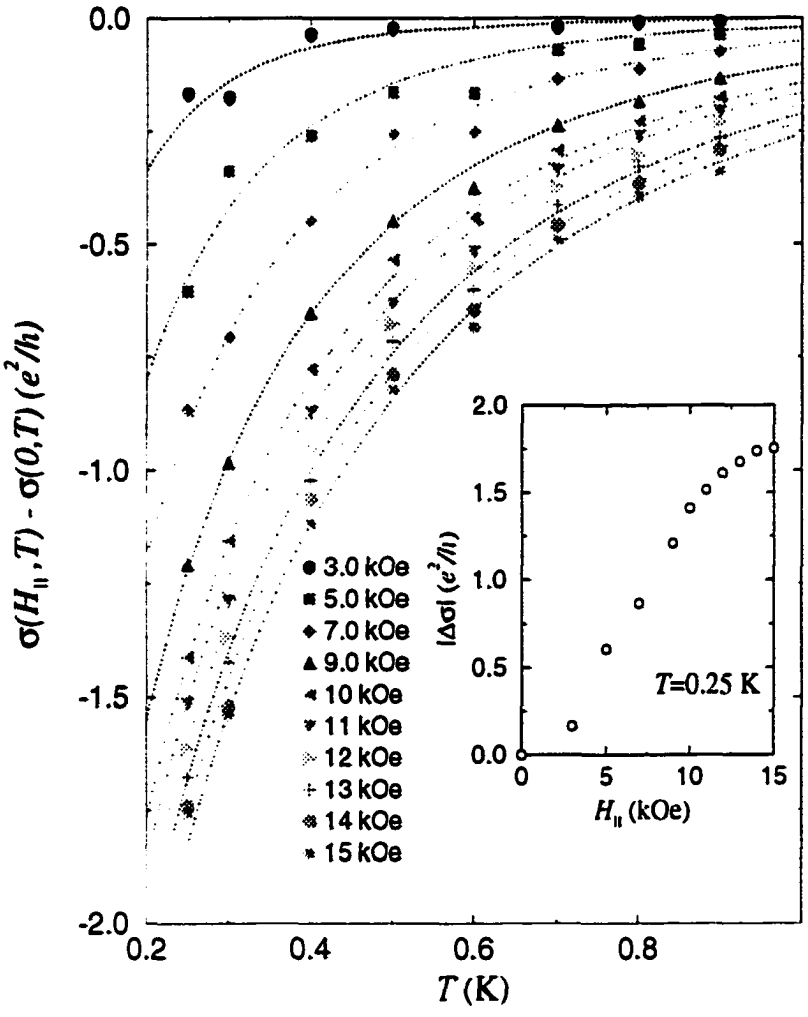

Figure 4.13: Magnetoconductivity $\Delta\sigma(H_{||},T) \equiv \sigma(H_{||},T) - \sigma(0,T)$ versus temperature T for several magnetic fields $H_{||}$ applied parallel to the plane of the electrons. In zero field the sample is in the conducting phase with an electron density $\delta = (n_s - n_c)/n_c = 0.10$. The dashed lines are guides to the eye. The inset shows the absolute value of the magnetoconductivity $|\Delta\sigma(H_{||},T)|$ versus $H_{||}$ at the lowest measured temperature, T =0.25 K. Note the rapid increase of $|\Delta\sigma(H_{||},T)|$ followed by saturation above $\approx$ 13 kOe.

resistance was 13.9 kOhm/□ at the lowest measured temperature, $T = 0.25$ K.

The magnetoconductivity, $\Delta\sigma(H_{||},T) = \sigma(H_{||},T) - \sigma(0,T)$, is shown in Fig-

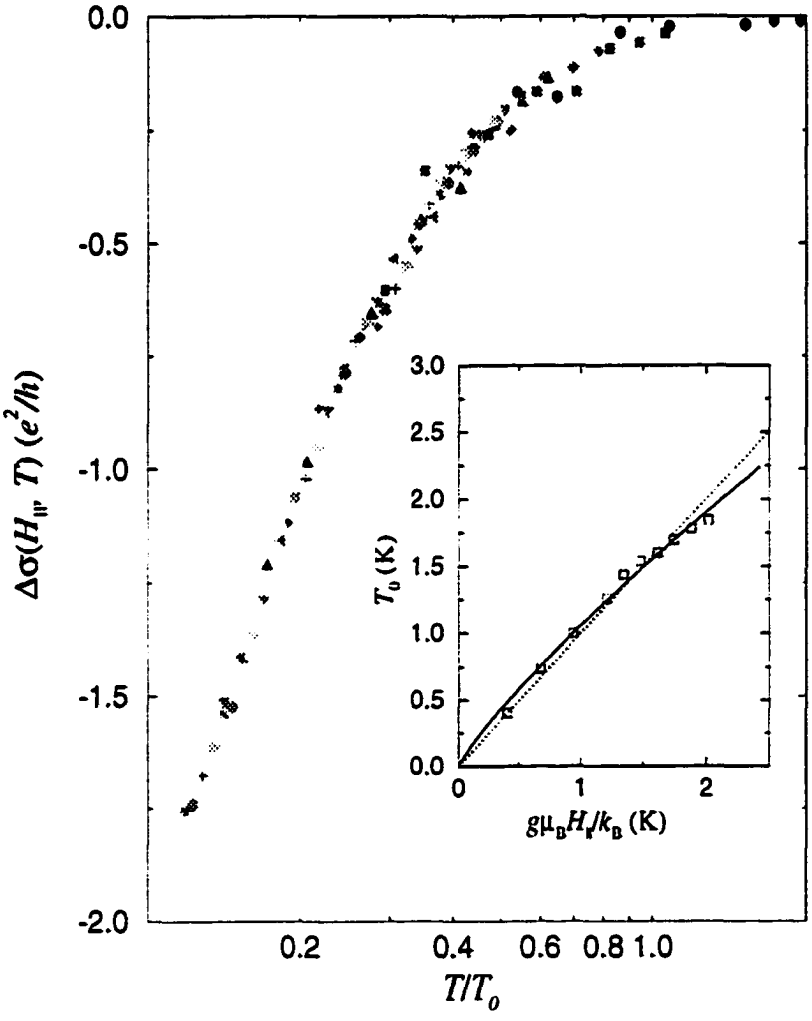

Figure 4.14: The magnetoconductance $\Delta\sigma$ as a function of T/T_0. The inset shows the scaling parameter T_0 plotted as a function of $g\mu_B H_{||}/k_B$. (Symbols for different fields, $H_{||}$, are the same as in Fig. 4.13). A power-law fit, shown by the solid curve, yields $T_0 \propto H_{||}^{\alpha}$ with $\alpha = 0.88 \pm 0.03$. The dotted straight line corresponds to $T_0 = g\mu_B H_{||}/k_B$; deviations from straight-line behavior are attributed to saturation at high fields (see text).

ure 4.13 as a function of temperature for various fixed values of parallel magnetic field. The magnetoconductance is negative, its absolute value increasing with applied field and with decreasing temperature. The noise for small $H_{||}$ derives from the sub-

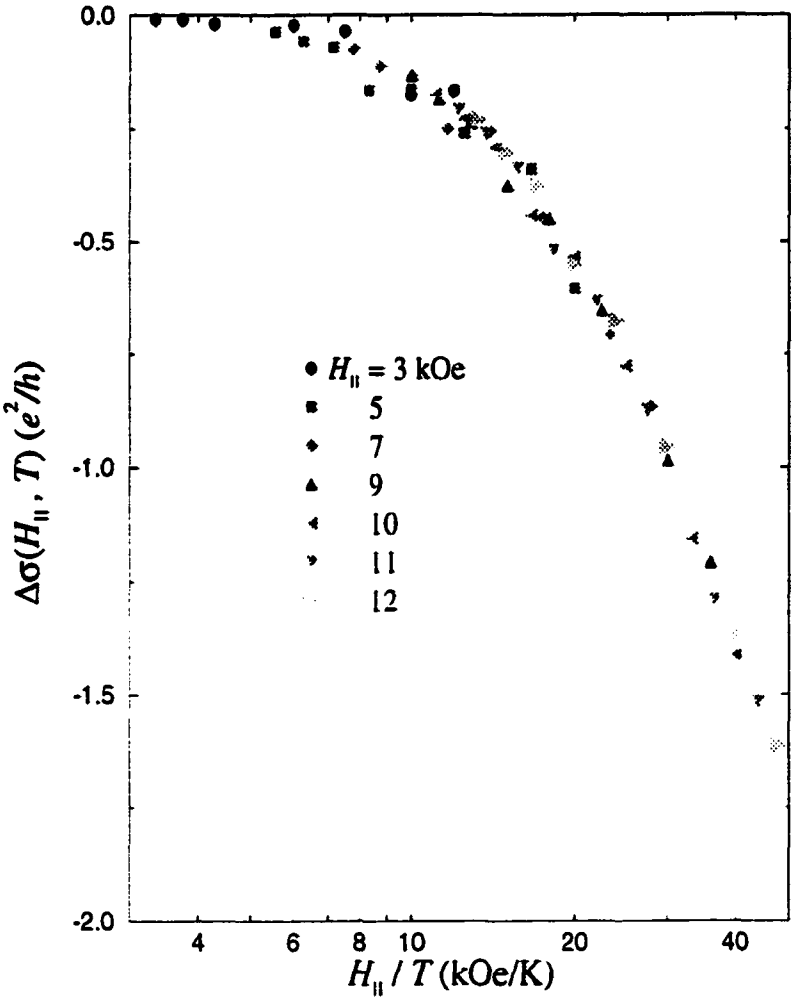

Figure 4.15: The magnetoconductance $\Delta\sigma(H_{||},T)$ as a function of $H_{||}/T$ for $H_{||} = 3$ to 12 kOe (see text).

traction of two large (and comparable) quantities, $\sigma(H_{||},T)$ and $\sigma(0,T)$. The inset to Figure 4.13 shows the absolute value of the magnetoconductivity as a function of $H_{||}$ at a temperature of 0.25 K. The absolute value of the magnetoconductance rises rapidly and begins to saturate above $\sim$ 13 kOe.

The data for $\Delta\sigma$ can be collapsed onto a single curve by applying a different multiplicative factor to the abscissa for each curve, as illustrated in Figure 4.14.

The scaling parameter T_0 is plotted in the inset as a function of the Zeeman energy, $g\mu_B H_{||}/k_B$ (in Kelvin). A power-law fit (shown by the solid curve) yields $T_0 \propto H_{||}^{\alpha}$, with $\alpha = (0.88 \pm 0.03)$. Note that H/T scaling of the form Equation (4.5) requires that $\alpha = 1$, corresponding to $T_0 = g\mu_B H_{||}/k_B$ (indicated in the inset by the dotted line). The deviation of α from unity may be associated with the saturation of the magnetoconductance at $H_{||} \geq 13$kOe shown in the inset to Fig. 4.13, where one might well expect the scaling to break down.[8] Therefore, the data sets at the three largest fields – for which the proximity of the scaling parameter T_0 to saturation is apparent – are excluded from the direct test of the H/T scaling presented in Figure 4.15. For in-plane fields in the range $H_{||}$=3...12 kOe, the magnetoconductance $\Delta\sigma(H_{||})$ is plotted as a function of the scaling variable H/T. For this range of magnetic fields and for an electron density fairly close to the critical density, the magnetoconductance scales well with $H_{||}/T$.

It should be noted in closing this Section that various scaling analyses were attempted for magnetotransport in a parallel magnetic field, and the magnetoconductivity scaling of Equation 4.5 is the only one-parameter scaling form consistent with the data. For example, the magnetoresistance $\Delta\rho(H_{||}, T)$ does not obey one-parameter scaling. The implications of the particular form of Equation 4.5 will be discussed in Chapter 5.

[8] It may also be associated with the possibility that H/T scaling does not strictly hold; for example, a weakly temperature-dependent prefactor may precede the scaling function f.

4.6 Suppression of the Conducting Phase by a Tilted Magnetic Field. Restoration of the "Ordinary" Magnetoresistance in a Perpendicular Field by Application of a Large In-Plane Magnetic Field

The results of the previous sections prompted the conjecture that the existence of the anomalous metallic-like behavior of a low-density 2D system is associated with electron spins, since this behavior disappears with the application of an in-plane magnetic field which only couples to spins. The perpendicular field, in turn, couples both to spins and to the orbital motion of electrons. Therefore, if electron spin coupling to a magnetic field is responsible for the quenching of the $H = 0$ conduction mechanism, then the latter should also be apparent in perpendicular field experiments. One may expect that orbital dynamics of electrons (that give rise to the quantum Hall effect) will also influence the magnetoresistance if the field is tilted from the in-plane direction.

These considerations stimulated the experiment which I am about to describe. Two Si MOSFET samples (a high-mobility sample P2 ($\mu_{4.2K}^{max} \approx 24,000$ cm^2/Vs) and a lower-mobility sample W01 ($\mu_{4.2K}^{max} \approx 8,000$ cm^2/Vs) (see Table 3.3 on page 31) were mounted on a rotating sample holder on the cold finger of the ^{3}He refrigerator.[9] The thermal contact between the cooling source – ^{3}He pot and the sample was provided by very thick copper wires which were coiled into springs to allow unimpeded rotation of the sample. With this arrangement, the lowest temperature of the sample was $T = 340$ mK.[10]

[9]The measurements of this Section were taken in A. D. Kent's lab at New York University.

[10]This temperature was read by the Dale 1kΩ RuO thermometer placed directly onto the sample chip.

Four-terminal dc transport measurements were taken as a function of magnetic field applied at different angles with respect to the plane of the electrons. The field was swept at a rate of 0.4 Tesla/min, and the voltage drop on the sample was recorded twice (on the way down and up) for both directions of current $I = \pm I_{exc}$, using the setup described in Section 3.2 on page 26 (see also Figure 3.3). The resistance was then calculated as the difference of voltage readings divided by $2I_{exc}$.[11] Excitation currents were between 0.1 nA and 10 nA, and care was taken to ensure measurements were in the linear $I - V$ regime by recording full IV curves at the base temperature at the beginning of the experiment.

First, the diagonal resistivity ρ_{xx} of sample P2 was measured in a perpendicular field ($\phi = \pi/2$) for a gate voltage that placed this sample in the conducting state at $H = 0$ (with a resistivity of $\approx$ 10 kΩ at 360 mK). Next, the resistivity ρ_{xx} of the relatively low-mobility sample W01 was measured in a perpendicular field. Both curves are shown on Figure 4.16 for comparison.

The electron density of the lower-mobility sample W01 was set at $n_s = 2.1 \times 10^{11}$ cm^{-2} by a gate voltage $V_g = 0.65$ V. Using the characterization technique described in Section 3.2. it was found that $n_s = 3.47 \times (V_g - V_T)$ with $V_T = 0.06 \pm 0.003$V. The sample is insulating at this electron density (as determined from the S-shaped IV characteristics measured at 0.36 K, and also from the resistivity change monitored during cooldown). No sign of conducting behavior was observed in sample W01 for any gate voltage in the range 0.5 V$< V_g <$10 V, so that disorder dominates (because the sample mobility is low) despite the fact that electron interactions are appreciable.

Let us first examine the magnetoresistance of sample W01. Khmelnitskii [56, 57] showed within the framework of scaling hypothesis for electron localization in

[11] I should note that this method is less accurate than deriving ρ from linear parts of IV characteristics employed in the previous sections. However, it was found adequate at ^{3}He temperatures, where contact problems discussed at the end of Section 3.2 were still manageable.

a magnetic field, that delocalized states located at the centers of Landau levels at high $H_\perp$ float up in energy as is $H_\perp$ decreased. As was also proposed by Laughlin in Ref. [59], the energy of delocalized states E_n changes with $H_\perp$ as follows:

$$E_n = \hbar\Omega(n + 1/2)(1 + (\Omega\tau)^{-2}), \tag{4.6}$$

where $\Omega = eH_\perp/mc$. At high $H_\perp$, $E_n \to \hbar\Omega(n + \frac{1}{2})$, which is equivalent to the statement that delocalized states are at the centers of Landau levels. At low $H_\perp$, Equation 4.6 gives:

$$E_n \to \hbar\Omega^{-1}(n + 1/2)\tau^{-2} \propto H_\perp^{-1}. \tag{4.7}$$

and as $H_\perp \to 0$, the energies E_n of all delocalized states (*i. e.* for all n) tend to infinity and the system becomes an insulator. A sketch of E_n curves versus $H_\perp$ is shown in Figure 4.17. In accord with these considerations, the resistance of our insulating sample W01 grows as $H_\perp \to 0$ – the extended states float upwards and away from the Fermi level. This results in the *negative* magnetoresistance ($\rho_{xx}(H) - \rho_{xx}(0) < 0$) exhibited by sample W01 (see Figure 4.16). As $H_\perp$ is increased, the extended states descend in energy. The Fermi level finds itself midway between centers of the 2nd and the 3rd Landau levels (so that 2 LL are filled) at approximately 32 kOe (where ρ_{xx} has a minimum). At 64 kOe only one LL is filled. At even higher magnetic fields the last extended state exits through the Fermi level, and we have an insulator again.[12] In strongly disordered GaAs/AlGaAs heterostructures (that are insulating at $H_\perp = 0$) similar behavior of resistivity with magnetic field – large *negative* magnetoresistance, transitions to quantum Hall conductor phases, and a transition to an insulator at high fields – has been observed by different groups [60, 47, 61, 62]. In

[12]It is clear that at different electron densities (hence, different positions of the Fermi level) one can end up seeing different numbers of resistivity minima (and different number of field-induced transitions). If $E_f < min(E_n)$, where E_n is from Equation 4.6, the sample will be an insulator at any $H_\perp$. See Figure 4.17.

contrast, the high-mobility sample P2 (see lower curve in Figure 4.16), which is in the anomalous conducting phase at $H = 0$, displays an anomalous magnetoconductance in a perpendicular magnetic field $H_\perp$. We notice that the large negative low-field magnetoresistance is absent in this case, and there is a substantial enhancement of the resistivity as $H_\perp$ is increased (around $\approx$ 15 kOe) which is overwhelmed by the orbital dynamics leading to $\nu = 1$ and 2 quantum Hall minima at higher H. The "anomalous peak" of the resistivity grows with decreasing temperature, as shown in earlier measurements of Pudalov *et al.* [58] on similar samples at similar electron densities at $T = 35$ mK. This enhancement of ρ_{xx} is in stark disagreement the "floating up" of extended states (see discussion preceding Equation 4.6), and has been a puzzle for several years. This anomaly has only been seen in systems undergoing the unexpected $H = 0$ MIT - high-mobility SiMOS devices [58]. However, the dramatic increase of resistivity that high-mobility MOSFETs exhibit in a *parallel* field (see Section 4.4 and Ref.[43]), suggests strongly that both effects are of the same origin. This can be tested by varying the angle between the field and the 2D electron layer and measuring the resistivity ρ_{xx} of high-mobility sample P2.

The result of this experiment is shown in Figure 4.18. For all angles between the applied field and the plane of the electrons, $\rho_{xx}(H)$ follows approximately the same curve up to some value of magnetic field, above which orbital effects leading to QH oscillations become dominant. The resistivity deviates from the "main" curve at smaller magnetic fields as the angle between the field and the plane is increased. This occurs simply because at a given total field, the larger ϕ the larger the perpendicular component, which causes stronger orbital effects. We note that small differences in $\rho_{xx}(H)$ at $H \sim 10$ kOe are associated with the emergence of a QHE minimum at filling factor $\nu = 6$[58], which deepens as the perpendicular component of the field gets larger. Also, the minimum at $\nu = 4$, masked by the resistivity peak in a perpendicular

field, becomes resolved in a tilted field at $\phi = 16.5°$ (notice a local resistivity minimum at about 40 kOe in Figure 4.18) due to the widening of spin splitting produced by a parallel magnetic field component. The most important feature of these dependences, however, is that the magnetoresistance is the same at all angles up to some field above which it is overwhelmed by orbital effects. The anomalous $H = 0$ conducting phase is thus suppressed in the same manner by a magnetic field applied at any angle.

It was already noted in Section 4.4 that magnetic field suppression of the anomalous conducting state cannot be attributed to a simple shift of the critical electron density. With the added capability to rotate the sample in a magnetic field in the ^{3}He system, thereby controlling both directions of the field independently, we verified explicitly that a magnetic field does not drive the sample into the insulating phase by simply reducing the electron mobility[13], or by reducing the electron density below its critical value. Figure 4.19 shows $\mu_{T=4.2\ K}$ of high-mobility sample P2 as a function of electron density in $H = 0$ and in the presence of a parallel magnetic field, $H_{||}$=30 kOe. These data establish that the mobility is essentially unaltered by a magnetic field. In the inset to Figure 4.19 I replot the resistance as a function of the perpendicular magnetic field component, $H_\perp = H\sin\phi$, for four different fixed angles with respect to the electron plane[14]. The QHE minima occur at the same $H_\perp$ for all angles, corresponding to different values of the total field. This observation establishes that the magnetic field does not change the density of 2D electrons. The dramatic growth with angle of the ρ_{xx} maximum at $H_\perp \sim 15$ kOe can be understood by recalling that the $H = 0$ conducting state is quenched independently of the field orientation: at a fixed $H_\perp \approx 15$ kOe, the total field increases with decreasing ϕ, $H = H_\perp / \sin\phi$, driving the

[13]The disappearance of the conducting phase with increasing disorder was first shown by Kravchenko *et al.* [6]

[14]Note that the parallel field, $H_{||} = H\cos\phi$, varies along each curve and is different for different angles ϕ.

sample closer to the insulating state.

It is very interesting to note that, in fact, *the only* role of the parallel field is to quench the conducting phase in the vicinity of $H = 0$. The parallel field component as large as 30 kOe produces no effect on transport in the quantum Hall regime, which is evident from the fact that all data collapse onto a single curve at sufficiently strong $H_\perp$ in the inset to Figure 4.19. Not only are the positions of the QHE minima unaltered by the in-plane field, but the overall behavior (once the $H = 0$ conducting mechanism has been quenched) is also insensitive to it.

Lastly, using the angle-dependent data, it becomes possible to map out the low-$H_\perp$ magnetoresistance in the "quenched" state. This can be done in the following way. The quenching of the anomalous phase, as we have shown above in this Section, is produced by the total magnetic field. We can therefore construct the resistivity $\rho_{xx}^{quenched}(H_\perp)$ in the "quenched" state by simply noting the $\rho_{xx}(H_\perp)$ dependence in a *large, fixed total field* H. This dependence is marked in Figure 4.16 by closed diamonds. We can immediately see that the magnetoresistivity has become negative at low $H_\perp$, and that the anomalous peak of the resistivity in $H_{||} = 0$ case has been removed. In the "quenched" state, high-mobility Si MOSFETs display the familiar reentrant behavior found in disordered, weakly interacting GaAs/AlGaAs heterostructures (see, *e.g.*, Figure 2 in Ref. [60]): the system has an initial large negative magnetoresistance, exhibits the quantum Hall effect at $\nu = 2$ and 1, and becomes again insulating above $H \simeq 42$ kOe[15].

To conclude this section, I summarize the main qualitative results of the tilted-field experiments: A magnetic field suppresses the anomalous $H = 0$ conducting phase in high-mobility silicon MOSFETs independently of the angle between the field and the plane of the electrons, thereby firmly establishing that the suppression of this phase is

[15]However, the initial decrease in resistivity is considerably less sharp than in disordered GaAs/AlGaAs.

associated only with the electrons' spins. In the presence of a parallel field sufficiently large to quench the anomalous conducting phase in high-mobility silicon samples, the resistivity exhibits as a function of perpendicular field all the familiar features found in disordered, low-mobility GaAs/AlGaAs heterostructures [60, 47, 61, 62]: a giant negative magnetoresistance at low $H_\perp$, the quantum Hall effect (QHE) at low Landau level filling factors, and insulating behavior at higher $H_\perp$. The suppression of the anomalous conducting phase is not associated with a simple change in mobility or electron density, both of which are essentially unaltered by the magnetic field.

This concludes the Chapter in which I reported the main experimental findings of this work. In the next Chapter, these findings will be discussed and compared to existing theoretical models, and to very recent results by other groups on the $H = 0$ MITs in other strongly interacting 2D systems.

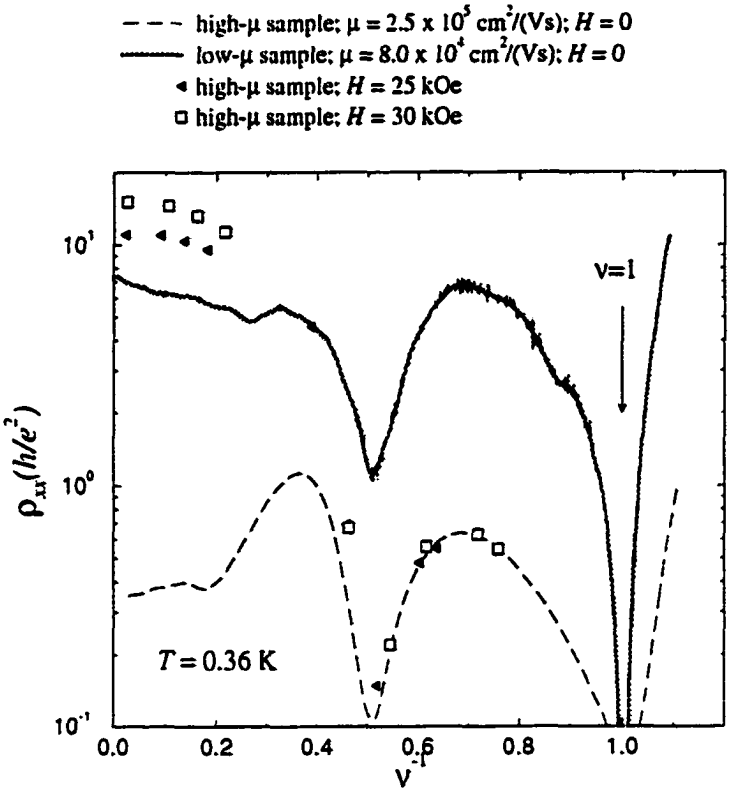

Figure 4.16: Resistivity of two samples with electron densities $n_s = 2.1 \times 10^{11}$ cm^{-2} (W01 - dashed line), and $n_s = 1.0 \times 10^{11}$ cm^{-2} (P2 - solid line) measured in a perpendicular field at $T = 0.36$ K, plotted as a function of an inverse filling factor ν^{-1} (which is proportional to $H_\perp$). The lower-mobility sample has an appreciable negative magnetoresistance consistent with the model of Ref. [56, 57]: extended states descend from infinity as the magnetic field increases from zero (see Equation 4.6). On the other hand, the higher-mobility sample (dashed line) behaves anomalously below $\sim$ 15 kOe: contrary to the expected insulating behavior, the resistivity drops by almost a factor of 4 at $T = 0.36$ K (a factor of 500 at 30 mK [58]), and approaches a finite value at $H = 0$.

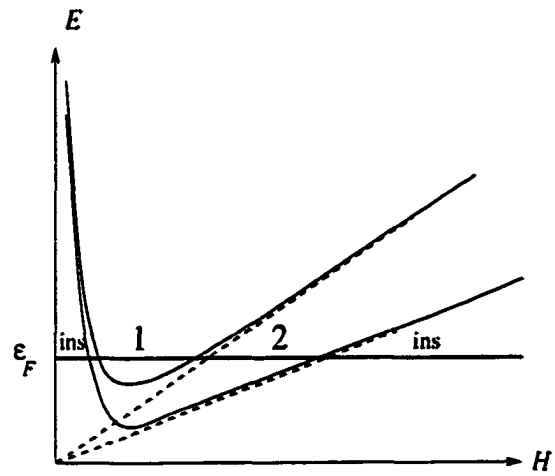

Figure 4.17: The extended electronic states follow the centers of LLs at large magnetic fields. At small fields, the extended states float up in energy with decreasing field. Depending on the position of the Fermi level, one observes different series of field-induced transitions in a 2D system with increasing $H_\perp$.

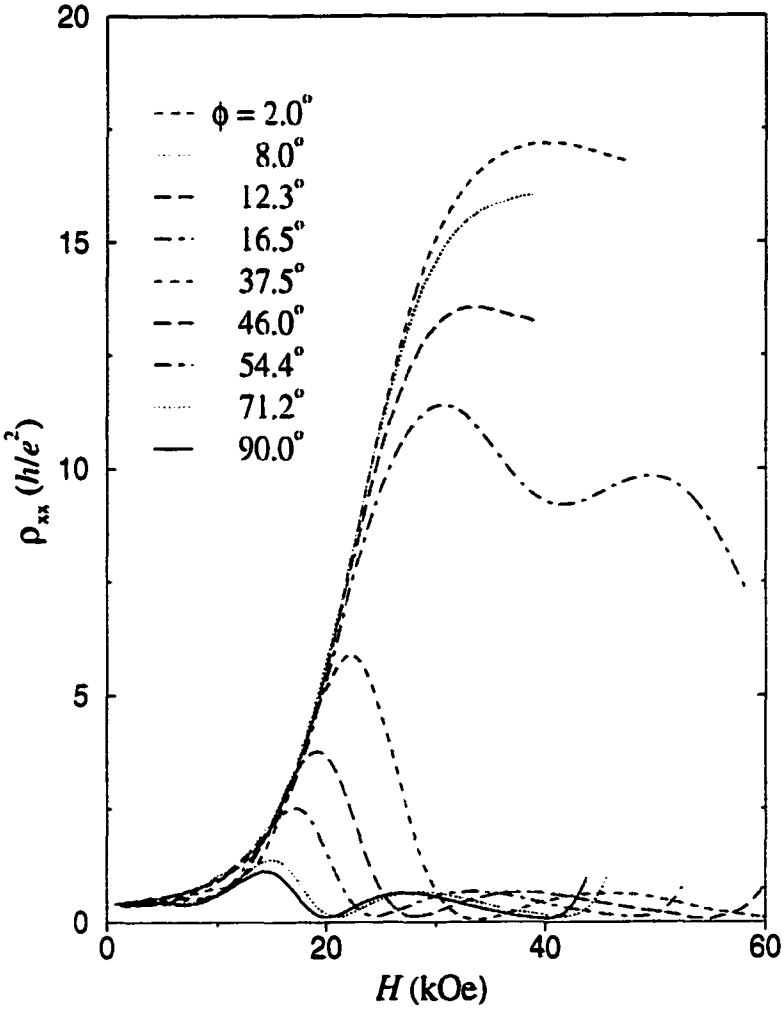

Figure 4.18: Resistivity as a function of the total magnetic field for a high-mobility sample P2, at $T = 0.36$ K and $n_s = 1.0 \times 10^{11}$ cm^{-2} for nine angles ϕ between the magnetic field and the inversion layer. ρ_{xx} deviates from the "main" curve at smaller magnetic fields as ϕ is increased.

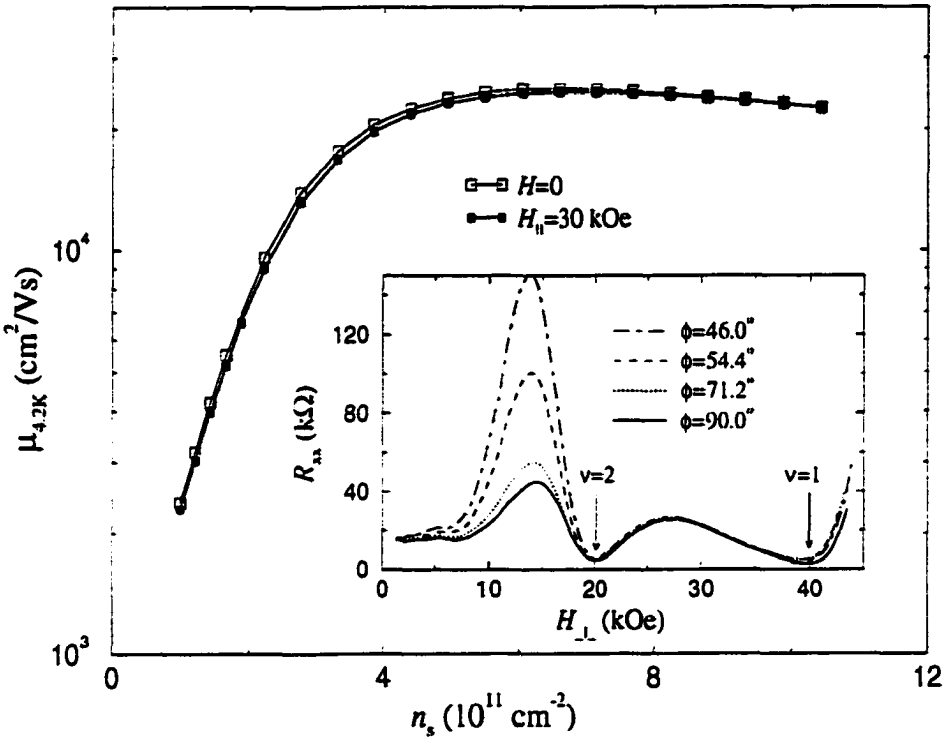

Figure 4.19: Mobility *vs* electron density for sample P2 at $T = 4.2$ K in zero magnetic field (open symbols) and $H_{||} = 30$ kOe (closed symbols). The inset shows R_{xx} as a function of $H_{\perp}$ for four angles between the field and 2D plane; $T = 0.36$ K and $n_s = 1.0 \times 10^{11}$ cm^{-2}. The positions of the minima do not change with the parallel field component, implying that the actual electron density is constant.

Chapter 5

THE SIGNIFICANCE OF EXPERIMENTAL FINDINGS AND COMPARISON WITH THEORY.

In this Chapter I compare – where possible – the experimental results with existing theoretical models. Unresolved issues and further experimental work that may clarify them are also discussed.

5.1 The scaling exponents: diverging correlation time versus phonons.

Let us discuss the significance of the elecric-field scaling analysis in Section 4.2. One important assumption of the scaling equation 2.16 is that the electron "temperature",

$T_E \sim eEL_E$, associated with the field is set by the diverging correlation length and time in the vicinity of the critical point. An alternative mechanism that gives rise to an electron temperature higher than the lattice temperature is phonon heating. At low T, phonons are capable of carrying away the Joule power of the electric field at a rate $P_{ph} \propto T^{*\theta}$ with $\theta = 4 \ldots 5$ [63] for the case of phonon radiation in GaAs/AlGaAs, and $\theta \approx 6$ in 2D layers in Si MOSFETs [63]; T^* is the effective electron temperature set by the phonon radiation rate. Thus, our measurements beyond the ohmic regime give information about the response to the electric field near the quantum critical point only if [26]:

$$T_E > T^* \tag{5.1}$$

At the critical point the resistivity is scale-independent, and therefore, from the equilibrium condition $P_{Joule} \equiv E^2/\rho = P_{ph}$, we obtain: $E^2 \propto T^{*\theta}$. Thus the condition 5.1 may not be satisfied at low electric fields: $T^* \propto E^{2/\theta} \approx E^{1/3}$, while $T_E \propto E^{z/(z+1)} = E^{1/2}$ if $z = 1$. The influence of phonon heating could be reflected in the somewhat low value of $z \approx 0.8$ [41] determined experimentally in Section 4.2.

Since the crossover between the two regimes discussed above has not been studied near the $B = 0$ transition in Si MOS devices, the following experiment could be proposed to distinguish between phonon heating effects and the quantum-critical response to an electric field. The power-law dependences of the effective electron temperature (T^* for phonons; T_E for quantum-critical response) should be obeyed in the immediate vicinity of the transition, *i.e.* where the resistivity has no electric-field dependence. For the same reason, measurements of resistivity dependences on T and E at the transition are not capable of yielding parametric $T(E)$ dependences, which could be used to distinguish between the two regimes. In other words, at the transition, the resistivity itself is not a good thermometer. On the other hand, the derivative $d\rho/dn_s$ evaluated at $n_s = n_c$ is extremely sensitive to temperature or

electric field[1]. Fitting the parametric $T(E)$ dependence — in which T is defined as the temperature for which the value of $d\rho/dn_s$ measured in the ohmic regime is equal to the value of $d\rho/dn_s$ measured as a function of E at low bath temperature — to a power law with exponent $z/(z+1)$, should allow the identification of the range of E within which the response to electric field is not affected by phonon heating.

5.2 Implications of the symmetry near the critical density.

The symmetry shown in Fig. 4.7 bears some resemblance to the behavior found for the resistivity near the quantum Hall liquid (QHL)-to-insulator transition in high mobility GaAs/AlGaAs heterostructures, where it has been attributed to charge-flux duality in the composite boson description [64]. The symmetry was shown in this case to hold for the entire nonlinear IV curve [65]. Approximate reflection symmetry of the IV curves was noted by van der Zant *et al.*[32] at the magnetic-field-induced superconductor-insulator transition in aluminum Josephson junction arrays; it has been suggested that this duality can be related to the symmetry between single charges in the superconducting phase and vortices in the insulating phase [66]. Approximate symmetry of the IV curves near the $H = 0$ transition in Si MOSFETs (apparent from Figure 4.1) suggested the possibility of superconducting mechanism [67] in the anomalous conducting phase.

However, the transport symmetry across the transition has been also interpreted within the phenomenological model of a "perfect metal" [68]. The assumption of the

[1] Wei *et al.* [37] used a similar quantity — $d\rho/dH$ as an thermometer to investigate the dependence of T^* on E at the transition between the quantum Hall plateaus in GaAs/AlGaAs heterostructure. Here H is a perpendicular magnetic field that tunes the transition.

model is that the one-parameter β-function introduced in Equation 2.5 on page 9 can be constructed in the vicinity of the $H = 0$ transition, even though the disorder is not the only parameter in a strongly-interacting disordered system. It is shown in Ref. [68] that the symmetry of the form of Equation 4.4 is a straightforward consequence of the linearization of $\beta(G)$ near the critical point G_c, where $G(L)$ changes sign.

It was noted in Section 4.3 that the range near the transition over which the reflection symmetry of the form of Equation 4.4 holds, decreases with decreasing temperature. The change in resistivity near the transition over which the symmetry holds remains approximately the same. If the $H = 0$ transition is a QPT, the shrinkage of the range of validity, $|\delta| \equiv |n_s - n_c|/n_c$, with decreasing temperature can be interpreted in terms of the dependence of the breadth of the quantum-critical region on temperature [68, 33] (see the definition in the footnote 12 on page 20). Indeed, the lower the temperature, the narrower the critical region, since the energy scale that measures the deviation from the critical point must be much smaller than k_BT. The question of the origin of the temperature dependence of the range near the transition over which the reflection symmetry holds is related to the low-T saturation of the resistivity on the conducting side of the transition. The data in Figure 2.3 were not taken to low enough T (or large enough electron density n_s) to reveal the saturation. Figure 5.1 illustrates this saturation. Below a certain characteristic temperature (different for different δ's), the resistivity dependence on temperature flattens out. It is not known what mechanism is responsible for the saturation. It is obvious, however, that the effect is not related to the experimental difficulty in cooling the 2D gas, since it occurs at much too high T's. It is plausible that the saturation is related to crossing the boundary of the critical region at low temperatures, which should occur at higher T for higher n_s — in qualitative agreement with the data in Figure 5.1. It is interesting to note that in another 2D system that has been recently found to

exhibit the metallic-like behavior — the hole gas in GaAs/AlGaAs — similar saturation of resistivity on the conducting side of the transition has been observed [69]. The question whether this saturation is quantitatively consistent with the limits of the critical region, or whether it is governed by entirely different physics is open and needs further study.

5.3 Magnetic-field suppression of the anomalous conducting phase.

It has been shown in Chapter 4 that the conducting phase can be suppressed by the application of a magnetic field, and that the suppression is independent of the field direction. The tilted-field experiment described in Section 4.6 showed that, together with the restoration of the "normal" (that is, strongly insulating) temperature dependence in the "quenched" state, the low-field anomaly in the magnetoresistance $\rho_{xx}(H_\perp)$ is suppressed by the application of a sufficiently strong in-plane magnetic field. We have shown, therefore, that the existence of the anomalous conducting state is intimately related to the existence of the anomalous magnetoresistance, inconsistent with the floating-up of the extended states. It is interesting that even before the observation of the $H = 0$ conducting state in high-mobility Si MOS devices, Shashkin *et al.* [70] constructed the low-temperature phase diagram of density and perpendicular magnetic field, and observed in the same system above a certain electron density that the extended states do not float up in energy indefinitely upon lowering the magnetic field.

The important consequence of the angle-independent suppression of the conducting phase is that the valleys peculiar to the inversion layers in Si probably do not

play an important role. According to Ref.[40], a field applied parallel to the plane of the 2DES in silicon MOSFETs does not affect the splitting of the two conduction band valleys. This splitting is enhanced in a perpendicular field due to exchange interaction, and is therefore expected to be a function of field orientation. The absence of any angular dependence implies that valley-splitting is not responsible for the suppression of the low-temperature conducting phase by a magnetic field. Since the valley spiting is thus an unlikely factor in the existence of the $H = 0$ phase, we arrive at the important conclusion that it is the electrons' spin that plays a crucial role.

The latter is further indicated by the observation of the H/T scaling of the magnetoconductance at the transition. Let us consider the scaling with the field in greater detail. For a weakly interacting 2D system, Lee and Ramakrishnan expect [55] a negative $|S_z| = 1$ triplet channel contribution to the conductance that is only a function of H/T in two dimensions:

$$\sigma(H,T) - \sigma(0,T) = -e^2/(4\pi^2\hbar)FG(\mu_B g H/k_B T). \tag{5.2}$$

where F is related to screening (see Equation 2.10 on page 13), and $G(x) = 0.084x^2$ for $x << 1$. For the case of an in-plane magnetic-field the equation above gives the total conductivity dependence on the magnetic field, since the localization contribution (that depends on $H_\perp$) is absent. This result should not be applicable to our case of strong electron-electron interactions; however, Sachdev showed [33] that, quite generally, in the vicinity of the quantum critical point of a system with a conserved spin the change of conductivity in response to a magnetic field $H_\parallel$ is only a function of $H_\parallel/T$. It has also been pointed out [71] that one should expect one-parameter scaling at the transition, since the energy scale that measures the deviation from the critical point is infinitesimal, and the conductivity should be described fully by the interplay between the field energy and the temperature.

Extending earlier work [72, 73], Castellani *et al.* [74] demonstrated that in the presence of strong Coulomb interactions, at low disorder, a 2D system can be metallic at the lowest temperatures, and that the low-field magnetoresistance can be written in the form:

$$\sigma(H,T) - \sigma(0,T) = -0.084e^2/(\pi h)\gamma_2(1+\gamma_2)(\mu_B g H/k_B T)^2, \qquad (5.3)$$

where γ_2 is a coupling parameter that may depend on temperature. This result may not be strictly valid near the transition, since it has been derived for the case of low disorder (*i.e.* resistivity small compared to h/e^2). It is consistent with H/T scaling in the case of weakly temperature-dependent coupling γ_2.

The observation of the comparability of Zeeman energy and thermal energy that destroy the low-temperature $H = 0$ conducting phase points to the fact that spin-orbit interactions are not important in driving the transition. A spin-orbit mechanism in a 2D system with broken symmetry produced by the confining potential well [75] has been proposed. Our estimate of the characteristic magnetic field that is associated with the electric field of the confining potential E. $H \sim v_F E/c$, gives a very small value incompatible with the characteristic field that destroys the conducting phase ~ 2 Tesla.

How small a magnetic field is needed to drive the system insulating is a question that is not fully resolved. The resistivity curves in a small magnetic field (which partially quenches the $H = 0$ conducting mechanism) $H_{||} = 5$ kOe in Figure 4.9 on page 51, change the behavior to that characteristic of an insulator only below a certain electron temperature. There is some evidence [6] that qualitatively similar increase in ρ with decreasing T (and the breakdown of scaling) at sufficiently small temperatures is observed in zero field in lower-mobility samples, in which the conducting state is not fully developed. Since the parallel magnetic field can be thought of as a means to partially "turn off" the interactions that are presumably responsible

for the conducting behavior, this question is related to whether there is a minimum interactions-to-disorder ratio that is sufficient for the system to scale to a metal in the limit of $T \to 0$. The latter has been studied in some detail by tuning the disorder by the application of a substrate bias in Ref. [76], but needs a more systematic approach: the conducting phase should be studied as a function of decreasing Coulomb interactions at a fixed amount of disorder. The experimental difficulty of separating the two accounts for the unsatisfactory understanding of this problem.

5.4 Concluding remarks

The existence of a conducting phase in strongly-interacting two-dimensional systems has been confirmed in p-GaAs/AlGaAs [69, 77] and in holes gases in Si/SiGe heterostructures [78]. In these systems, the interactions between carriers are very strong: the conducting phase in p-GaAs/AlGaAs was found at hole densities on the order of 10^{10}cm^{-2}, at which $\epsilon_F \approx 0.5 \ldots 3.7$ K, and the ratio of the interactions to Fermi energy, $\epsilon_{pp}/\epsilon_F \approx 24 \ldots 9$ [69]; in p-Si/SiGe heterostructures the transition occurs at hole densities on the order of 10^{11}cm^{-2}, and $\epsilon_F \approx 0.5$ meV, $\epsilon_{pp} \approx 6.5$ meV [78]. The interactions, therefore, provide the dominant energy scale in all systems in which the unexpected $H = 0$ conducting phase has been seen. Our experiments in magnetic field support the possibility that the spin-dependent part of the interactions between carriers is the key ingredient necessary for the conducting state. Similar observations of the suppression by an in-plane magnetic field has been recently made in p-GaAs/AlGaAs [77]. This suggests a quite general mechanism, independent of details peculiar to these two-dimensional systems (such as holes or electrons, presence of multiple valleys, the form of the confining potential).

The most important question that has no accepted answer up to now is the mi-

croscopic nature of the state. Transport measurements which are reported in this Thesis give many properties of the conducting state and the conductor-to-insulator transition, but do not elucidate the microscopic physics. There is no doubt that other experiments will be performed in the near future by different groups, of which the measurements that probe the density of states seem to be potentially very interesting: capacitance measurements at zero-field, similar to that of Ref. [79]; experiments on strongly interacting double 2D layers, similar to Ref. [80]; and measurements of the tunneling density of states.

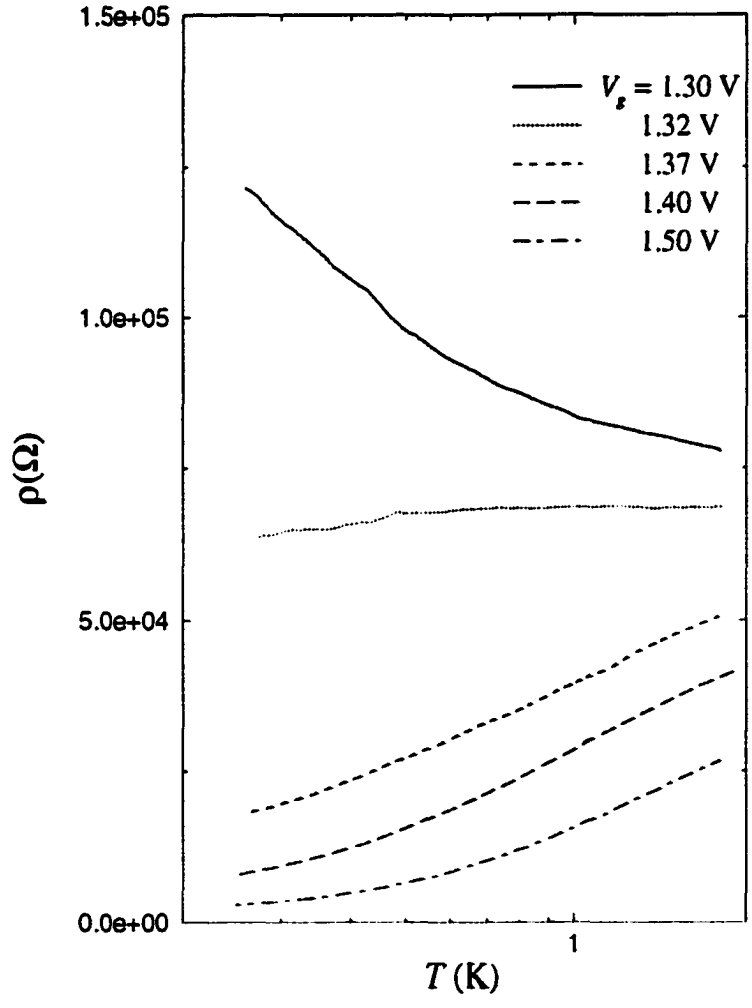

Figure 5.1: Resistivity of a high-mobility sample P2 as a function of temperature. Each curve corresponds to a different electron density n_s set by the gate voltage ($V_g = 1.33$ V is very close to critical. Note the apparent low-temperature saturation of $\rho(T)$ on the conducting side of the transition. which occurs at higher temperatures for higher values of V_g.

Bibliography

[1] T. Ando, A. B. Fowler, and F. Stern. *Rev. Mod. Phys*, 54:437, 1982.

[2] T. Maurice Rice. *Nature*. 389:916. 1997.

[3] E. Abrahams. P. W. Anderson, D. C. Licciardello. and T. V. Ramakrishnan. *Phys. Rev. Lett.*, 42:673, 1979.

[4] R. E. Prange and S. M. Girvin, editors. *The Quantum Hall Effect.* Springer, Berlin, 1987.

[5] Robert L. Willett. *Advances in Physics*. 46:447. 1997.

[6] S. V. Kravchenko. G. V. Kravchenko. J. E. Furneaux. V. M. Pudalov. and M. D'Iorio. *Phys. Rev. B*. 50:8039. 1994.

[7] L. P. Gor'kov, A.I. Larkin, and D. E. Khmelnitskii. *Pis'ma JETP*, 30:248, 1979.

[8] B. L. Altshuler, D. E. Khmelnitskii, A.I. Larkin, and P. A. Lee. *Phys. Rev. B*, 22:5142, 1980.

[9] S. Hikami, A. I. Larkin, and Y. Nagaoka. *Prog. Theor. Phys.*, 63:707, 1980.

[10] D. J. Bishop, R. C. Dynes, and D. C. Tsui. *Phys. Rev. B*, 26:773, 1982.

[11] G. Bergmann. *Phys. Rev. Lett.*, 48:1046, 1982.

[12] M. E. Gershenson and V. N. Gubankov. *Solid State Commun.*, 41:33, 1982.

[13] A. A. Abrikosov. *The Foundamentals of the Theory of Metals.* Elsevier Science, 1988.

[14] D. J. Thouless. *Phys. Rep.*, 13:93, 1974.

[15] L. Van der dries, C. Van Haesendonck, Y. Bruynseraede, and G. Deutscher. *Phys. Rev. Lett.*, 46:565, 1981.

[16] D. J. Bishop, D. C. Tsui, and R. C. Dynes. *Phys. Rev. Lett.*, 44:1153, 1980.

[17] M. J. Uren, R. A. Davies, M. Kaveh, and M. Pepper. *J. Phys. C.* 14:L395, 1980.

[18] F. W. Van Keuls, H. Mathur, H. W. Jiang, and A. J. Dahm. *Phys. Rev. B*, 56:13263, 1997.

[19] B. L. Altshuler and A. G. Aronov. *Zh. Eksp. Teor. Fiz.*, 77:2028, 1979.

[20] B. L. Altshuler, A. G. Aronov, and P. A. Lee. *Phys. Rev. Lett.*, 44:1288, 1980.

[21] M. D'Iorio, V. M. Pudalov, and S. G. Semenchinsky. *Phys. Rev. B*, 46:15992, 1992.

[22] S. V. Kravchenko, J. A. A. J. Perenboom, and V. M. Pudalov. *Phys. Rev. B*, 44:13513, 1991.

[23] V. J. Goldman, M. Santos, M. Shayegan, and J. E. Cunningham. *Phys. Rev. Lett.*, 65:2189, 1990.

[24] H. W. Jiang, R. L. Willett, H. L. Stormer, D. C. Tsui, L. N. Pfeiffer, and K. W. West. *Phys. Rev. Lett.*, 65:633, 1990.

[25] S. V. Kravchenko, W. E. Mason, G. E. Bowker, J. E. Furneaux, V. M. Pudalov, and M. D'Iorio. *Phys. Rev. B*, 51:7038, 1995.

[26] S. L. Sondhi, S. M. Girvin, J. P. Carini, and D. Shahar. *Rev. Mod. Phys.*, 69:315, 1997.

[27] A. F. Hebard and M. A. Paalanen. *Phys. Rev. Lett.*, 65:927, 1990.

[28] A. Yazdani and A. Kapitulnik. *Phys. Rev. Lett.*, 74:3037, 1995.

[29] Y. Liu, K. A. McGreer, B. Nease, D. B. Haviland, G. Martinez, J. W. Halley, and A. M. Goldman. *Phys. Rev. Lett.*, 67:2068, 1991.

[30] Peihua Dai, Youzhu Zhang, and M. P. Sarachik. *Phys. Rev. Lett.*, 66:1914, 1991.

[31] M. A. Paalanen, T. F. Rosenbaum, G. A. Thomas, and R. N. Bhatt. *Phys. Rev. Lett.*, 48:1284. 1982.

[32] H. S. J. van der Zant, F. C. Fritschy, W. J. Elion, L. J. Geerligs, and J. E. Mooij. *Phys. Rev. Lett.*, 69:2971. 1992.

[33] Subir Sachdev. *Zeitschrift Phys. B*, 94:469, 1994.

[34] S. Chakravarty. B. I. Halperin. and D. R. Nelson. *Phys. Rev. B*, 39:2344, 1989.

[35] S. Sachdev and J. Ye. *Phys. Rev. Lett.*, 69:2411. 1992.

[36] L. W. Engel. D. Shahar, C. Kurdak, and D. C. Tsui. *Phys. Rev. Lett.*, 71:2638, 1993.

[37] H. P. Wei, L. W. Engel, and D. C. Tsui. *Phys. Rev. B*, 50:14 609, 1994.

[38] A. B. Fowler. F. F. Fang. W. E. Howard. and P. J. Stiles. *Phys. Rev. Lett.*, 16:901, 1966.

[39] H. Kohler and M. Roos. *Phys. Status Solidi (b)*, 91:233, 1979.

[40] R. J. Nicholas, K. von Klitzing, and Th. Englert. *Solid State Commun.*, 34:51, 1980.

[41] S. V. Kravchenko, D. Simonian, M. P. Sarachik, Whitney Mason, and J. E. Furneaux. *Phys. Rev. Lett.*, 77:4938, 1996.

[42] D. Simonian, S. V. Kravchenko, and M. P. Sarachik. *Phys. Rev. B*, 55:R13 421, 1997.

[43] D. Simonian, S. V. Kravchenko, M. P. Sarachik, and V. M. Pudalov. *Phys. Rev. Lett.*, 79:2304, 1997.

[44] D. Simonian, S. V. Kravchenko, M. P. Sarachik, and V. M. Pudalov. *Phys. Rev. B*, 57:R 9420, 1998.

[45] S. V. Kravchenko, D. Simonian, M. P. Sarachik, A. D. Kent, and V. M. Pudalov. *Phys. Rev. B Brief Reports*, 58:3553, 1998.

[46] W. Mason, S. V. Kravchenko, and J. E. Furneaux. *Surface Sci.*, 361/362:953, 1995.

[47] T. Wang, K. P. Clark, G. F. Spencer, A. M. Mack, and W. P. Kirk. *Phys. Rev. Lett.*, 72:709, 1994.

[48] D. Shahar, D. C. Tsui, M. Shayegan, R. N. Bhatt, and J. E. Cunningham. *Phys. Rev. Lett.*, 74:4511, 1995.

[49] L. W. Wong, H. W. Jiang, N. Trivedi, and E. Palm. *Phys. Rev. B*, 51:18033, 1995.

[50] S.-Y. Hsu and Jr. J. M. Valles. *Phys. Rev. Lett.*, 74:2331, 1995.

[51] D. G. Polyakov and B. I. Shklovskii. *Phys. Rev. B*, 48:11 167, 1993.

[52] D. Shahar, D. C. Tsui, M. Shayegan, J. E. Cunningham, E. Shimshoni, and S. L. Sondhi. *Solid State Commun.*, 102:817, 1997.

[53] J. K. Jain. *Phys. Rev. Lett.*, 63:199, 1989.

[54] V. M. Pudalov, G. Brunthaler, A. Prinz, and G. Bauer. *JETP Lett.*, 65:932, 1997.

[55] P. A. Lee and T. B. Ramakrishnan. *Rev. Mod. Phys.*, 57:287, 1985.

[56] D. E. Khmelnitskii. *Pis'ma Zh. Eksp. Teor. Fiz.*, 38:454, 1983.

[57] D. E. Khmelnitskii. *Phys. Lett. A*, 106:182, 1984.

[58] V. M. Pudalov, M. D'Iorio, and J. W. Campbell. *Surface Sci.*, 305:107, 1994.

[59] R. B. Laughlin. *Phys. Rev. Lett.*, 52:2304, 1984.

[60] H. W. Jiang, C. E. Johnson, K. L. Wang, and S. T. Hannahs. *Phys. Rev. Lett.*, 71:1439, 1993.

[61] R. J. F. Hughes, J. T. Nicholls, J. E. F. Frost, E. H. Linfield, M. Pepper, C. J. B. Ford, D. A. Ritchie, G. A. C. Jones, Eugene Kogan, and Moshe Kaveh. *J. Phys. Cond. Mat.*, 6:4763, 1994.

[62] D. Shahar, D. C. Tsui, and J. E. Cunningham. *Phys. Rev. B*, 52:R1, 1995.

[63] E. Chow, H. P. Wei, S. M. Girvin, and M. Shayegan. *Phys. Rev. Lett.*, 77:1143, 1996.

[64] Steven Kivelson, D.-H. Lee, and S.-C. Zhang. *Phys. Rev. B*, 46:2223, 1992.

[65] D. Shahar, D. C. Tsui, M. Shayegan, E. Shimshoni, and S. L. Sondhi. *Science*, 274:591, 1996.

[66] S. M. Girvin. *Science*, 274:524, 1996.

[67] P. Phillips, Y. Wan, I. Martin, S. Knysh, and D. Dalidovich. unpublished, preprint cond-mat/9709168.

[68] V. Dobrosavljevic, E. Abrahams, E. Miranda, and S. Chakravarty. *Phys. Rev. Lett.*, 79:455, 1997.

[69] Y. Hanein, U. Meirav, D. Shahar, C. C. Li, D. C. Tsui, and Hadas Shtrikman. *Phys. Rev. Lett.*, 80:1288, 1998.

[70] A. A. Shashkin, G. V. Kravchenko, and V. T. Dolgopolov. *JETP Lett.*, 58:220, 1993.

[71] V. Dobrosavljevic. private communication.

[72] A. M. Finkel'shtein. *Sov. Phys. JETP*, 57:97, 1983.

[73] C. Castellani, C. DiCastro, P. A. Lee, and M. Ma. *Phys. Rev. B*, 30:527, 1984.

[74] C. Castellani, C. DiCastro, and P. A. Lee. *Phys. Rev. B*. 57:R 9381, 1998.

[75] V. M. Pudalov. unpublished, preprint cond-mat/9707075.

[76] D. Popovic, A. B. Fowler, and S. Washburn. *Phys. Rev. Lett.*, 79:1543, 1997.

[77] M. Y. Simmons, A. R. Hamilton, M. Pepper, E. H. Linfield, P. D. Rose, D. A. Ritchie, A. K. Savchenko, and T. G. Griffiths. *Phys. Rev. Lett.*, 80:1292, 1998.

[78] P. T. Coleridge, R. Williams, Y. Feng, and P. Zawadzki. *Phys. Rev. B*, 56:R12 764, 1997.

[79] S. V. Kravchenko, V. M. Pudalov, and S. G. Semenchinsky. *Phys. Lett. A*, 141:71, 1989.

[80] J. P. Eisenstein, L. N. Pfeiffer, and K. W. West. *Phys. Rev. Lett.*, 68:674, 1992.

IMAGE EVALUATION TEST TARGET (QA-3)

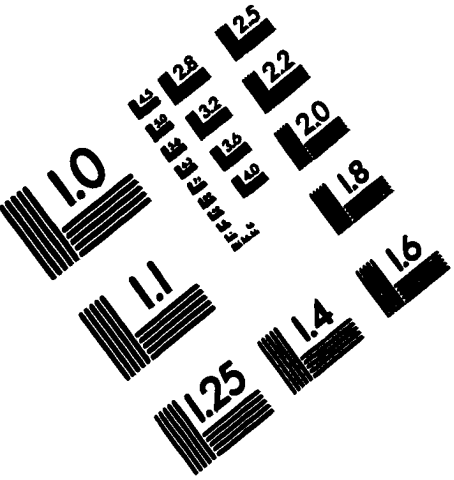

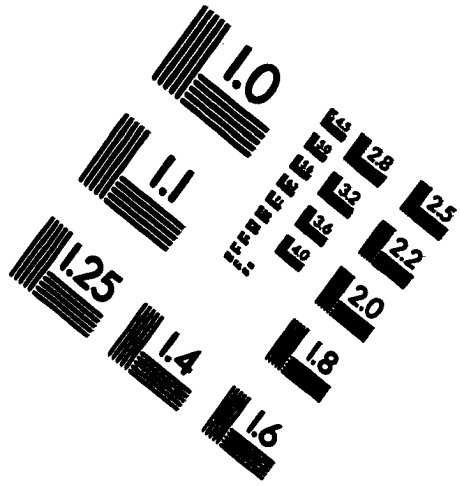

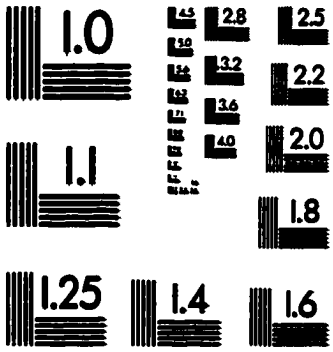

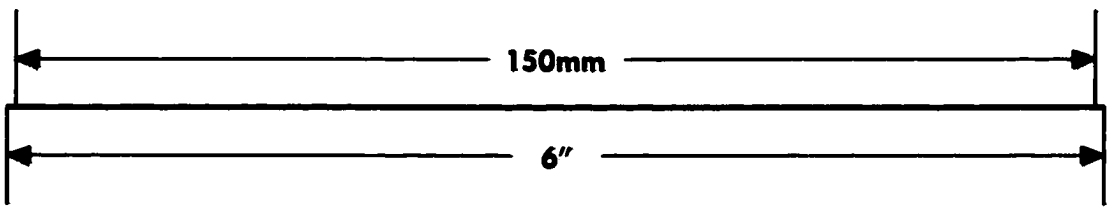

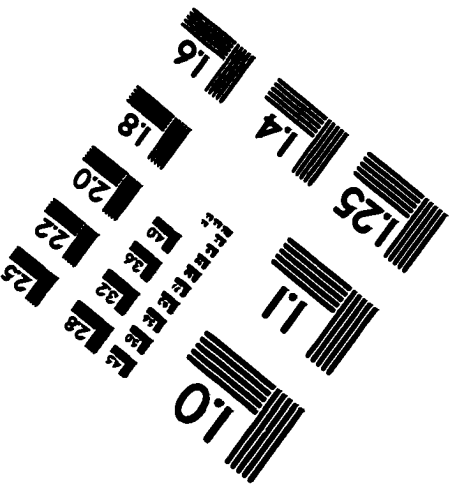

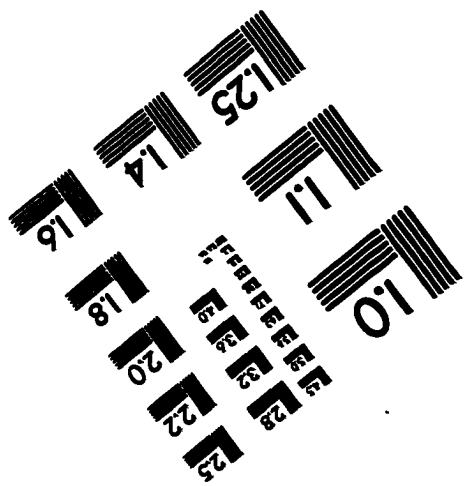

APPLIED IMAGE, Inc
1653 East Main Street
Rochester, NY 14609 USA
Phone: 716/482-0300
Fax: 716/288-5989